Journal of Palaeogeography, 2024, 13(4): 675–705 (00350)

Available online at www.sciencedirect.com

ScienceDirect

journal homepage: http://www.journals.elsevier.com/journal-of-palaeogeography/

Facies analysis and sedimentary environments

The "underfilled trinity model" of foreland basins revisited: reality or myth?

Xiu-Mian Hu [a,*], *Eduardo Garzanti* [b], *Juan Li* [a,1], *Marcelle BouDagher-Fadel* [c,1], *Giovanni Coletti* [b], *An-Lin Ma* [a], *Wen-Dong Liang* [a,b], *Wei-Wei Xue* [a]

[a] *State Key Laboratory of Mineral Deposits Research, Institute of Continental Geodynamics, School of Earth Sciences and Engineering, Nanjing University, Nanjing 210023, China*
[b] *Department of Earth and Environmental Sciences, Università di Milano-Bicocca, Milano 20126, Italy*
[c] *Department of Earth Sciences, University College London, Gower Street, London WC1E 6BT, UK*

Abstract The "*underfilled trinity*" model of foreland-basin stratigraphy was proposed based on the observation that the initial sedimentary stages along the western and northern front of the western and central Alps were represented by shallow-water carbonates (Calcaires à Nummulites) overlain by hemipelagic marls (Marnes Bleues) and capped by siliciclastic turbidites (Grès d'Annot). Subsequently, this model has been widely accepted and applied in foreland basins worldwide. We here re-investigated the Eocene-Oligocene sedimentary succession of the Western Alps to check its validity. Major geological features of this region include: i) the existence of a Cretaceous-Eocene unconformity spanning more than 25 Myr in the studied sections; ii) a virtually synchronous age of the Calcaires à Nummulites, Marnes Bleues, and Grès d'Annot formations across the Western Alps; iii) a long-term deepening-upward trend, from inner to outer ramp, documented by the Calcaires à Nummulites, followed by the pelagic Marnes Bleues and by the Grès d'Annot turbidites; iv) the provenance of the Grès d'Annot Formation from the Maures-Estérel Massif and/or Corsica-Sardinia block in the south, rather than from the Alpine orogen in the east. By integrating field observations, sedimentological, biostratigraphic, and provenance analyses, we found the Eocene "underfilled foreland" model too simplistic and inadequate to explain the basin evolution in the western Alpine region. Based on the alternative scenario proposed herein, the Annot and Barrême basins formed in the late Eocene (40-35 Ma) in an extensional/transtensional setting during a period of major change in tectonic stress fields across western Europe on the upper plate of the Apennine subduction.

Keywords Western Alps, Paleogene, Annot basin, Foreland-basin models, Flysch and molasse stages, Apenninic subduction

Received 17 April 2024; accepted 2 July 2024; available online 6 July 2024

* Corresponding author.
E-mail address: huxm@nju.edu.cn (X.-M. Hu).
Peer review under responsibility of China University of Petroleum (Beijing).
[1] Deceased.
https://doi.org/10.1016/j.jop.2024.07.001

1. Introduction

Whenever plates converge and two continental margins come into contact, a subsiding foreland basin is formed on top of the subducting plate along the front of a nascent collisional orogen (Dickinson, 1974). In most current tectonic models, foreland-basin subsidence is principally seen as an effect of lithospheric flexure in response to the orogen's load (Beaumont, 1981; DeCelles and Giles, 1996), although dynamic forces associated with plate subduction are generally dominant (Sinclair and Naylor, 2012; Garzanti *et al.*, 2021).

The stratigraphic evolution of a foreland basin was classically subdivided into an early underfilled stage of deep-marine sedimentation ('flysch'), followed by a late overfilled stage, characterized by coarser-grained, shallow-marine to non-marine clastic sediments ('molasse') (Covey, 1986; Heller *et al.*, 1988; Allen *et al.*, 1991). Largely based on studies of the Cenozoic foreland-basin succession of the western and northern central Alps in France and Switzerland, the initial underfilled stage has been subdivided into three substages (the *underfilled trinity* of Sinclair, 1997). Such a broad three-fold subdivision of depositional modes would correspond to three distinct stratigraphic units, envisaged as being superimposed in a typical foreland-basin succession and consisting of (from bottom to top): 1) shallow-water carbonates deposited on the foreland margin of the basin; 2) hemipelagic muds deposited offshore; and 3) siliciclastic turbidites accumulating in the deep-water trough adjacent to the orogenic margin of the basin.

Based on such a concept proposed for the Cenozoic foreland basin of the Western Alps, the rates of thrust advance and basin-fill migration were calculated and tested by numerical modelling (Ford *et al.*, 1999; Allen *et al.*, 2001; Kempf and Pfiffner, 2004). This contributed to validating the *underfilled trinity* hypothesis, which has been applied since then in the study of foreland basins worldwide. Examples include the Miocene basin in the Arabia-Anatolia collision zone of SE Turkey (Boulton and Robertson, 2007), the Triassic Sichuan Basin in front of the Longmenshan in western China (Li *et al.*, 2003), the Paleogene Himalayan foreland basin in Tibet (Zhang *et al.*, 2012), the Eocene south-Pyrenean basin in Spain (Huyghe *et al.*, 2012), and the Neogene foreland basin in western Taiwan (Yu and Chou, 2001).

However, such a rigid conceptual scheme adapts poorly to other foreland-basin systems. In the Himalayas, for instance, the rapid transition from trench deposits to deep-water turbidites fed from the Asian upper-plate margin is documented in middle Paleocene successions deposited on the toe of the lower-plate Indian passive margin (e.g., Sangdanlin and Mubala sections described in DeCelles *et al.*, 2014; Hu *et al.*, 2015, 2016; An *et al.*, 2021; Liu *et al.*, 2021). Such a transition is justified because the foreland basin initially originated at the site occupied by the Neotethyan trench during the previous phase of oceanic subduction (DeCelles *et al.*, 2014). Deep-water sedimentation, however, ceased only a few Myr after collision onset and, starting from the early Eocene until the present day, the Himalayan foreland basin hosted only fluvio-deltaic to continental molassic deposits (Garzanti, 2019a and references therein).

Because numerous variables control natural phenomena, every geodynamic setting is characterized by peculiarities associated with rheologies, geometries, and stress fields that inevitably differ from place to place. It is thus always necessary, although seldom straightforward, to filter what is specific to a local region from processes of broader significance. With this in mind, we have revisited the well-studied Paleogene outcrops beautifully exposed in the Western Alps, to verify whether the stratigraphic observations and inferences made in the past, including the *underfilled trinity* hypothesis, can be indeed considered as a valuable tectono-stratigraphic model for foreland basins worldwide or, instead, whether, and to what extent, the significance of aspects unique to that sedimentary basin have been unduly stretched and erroneously considered of universal validity (Schumm, 1998).

This article aims to re-investigate the classic Eocene-Oligocene succession of the Western Alps, illustrated by an original set of integrated field observations and sedimentological, biostratigraphic, and provenance data. The tectonic nature of the Eocene-Oligocene sedimentary basin is finally discussed.

2. Geological framework

2.1. The Western Alps

The Alpine collisional orogen formed during Cretaceous-Cenozoic convergence between the European continent and the Adria microplate that culminated in the Paleogene, with the final closure of the intervening Alpine branch of the Neotethys Ocean (Schmid *et al.*, 1996; Stampfli *et al.*, 1998; Handy *et al.*, 2010). The Western-Central Alps transect consists of

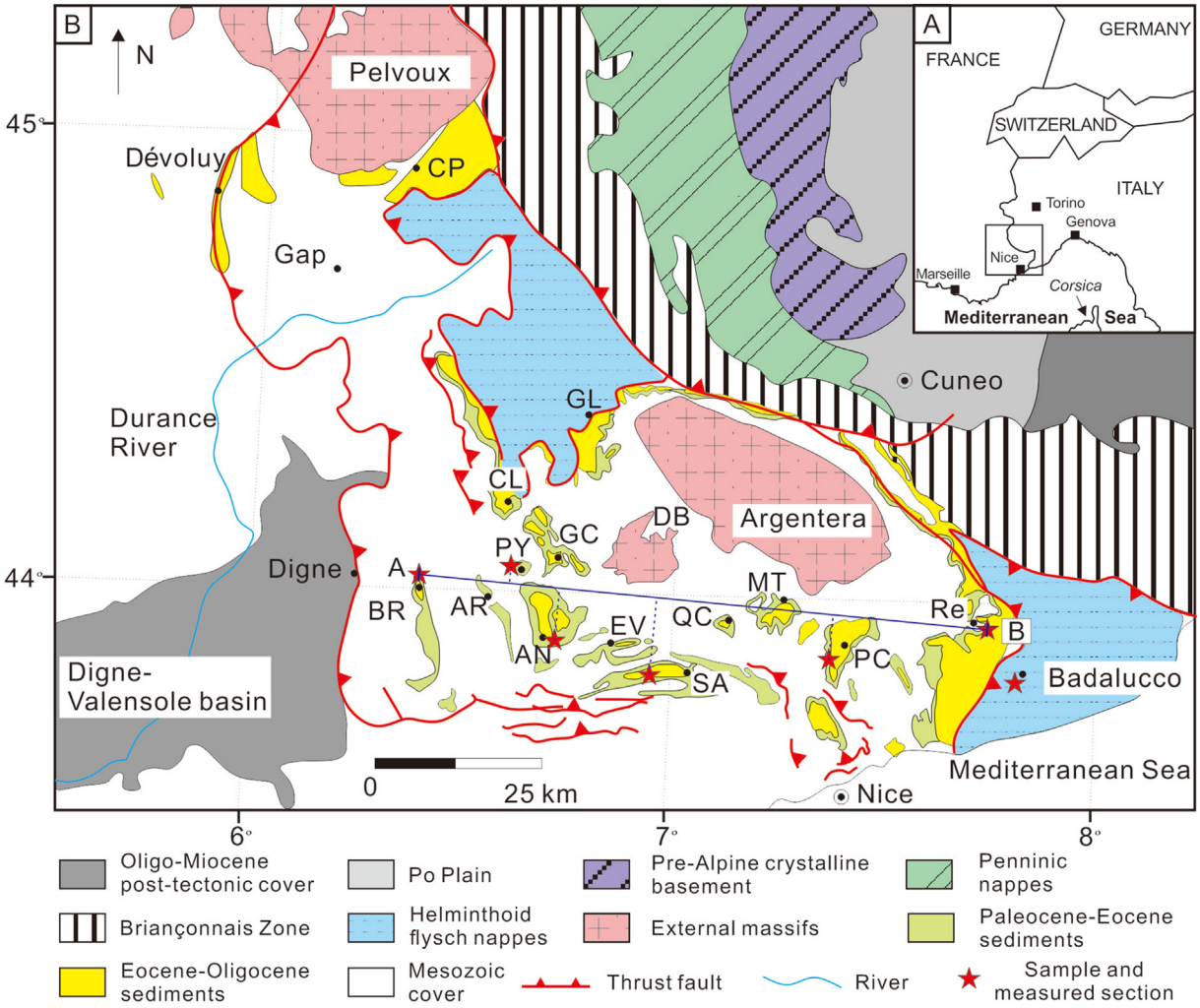

Fig. 1 Simplified geological map showing the studied Eocene-Oligocene sedimentary basins and the Cretaceous deep-water basin near Badalucco in the Western Alps (modified from Sinclair, 1997). The rectangle in Fig. 1A outlines the study area, enlarged in Fig. 1B. AN-Annot; AR- Argens; BR-Barrême; CL-Chaluty; CP-Champsaur; DB-Dôme de Barrot; EV-Entrevax; GC-Grand Coyer; GL-Gialorgus; MT-Menton; QC-Quatre Cantons; PC-Peira Cava; PY- Peyresq; SA-St Antonin; Re-Realdo. The lithostratigraphic units in the section from A to B can be found in Fig. 4.

several tectonic domains, which include, from southeast to northwest (Fig. 1; Schmid *et al.*, 2004; Garzanti *et al.*, 2004): i) the basement and cover strata of the Southern Alps; ii) the Insubric Line and associated Eocene-Oligocene magmatic rocks (Periadriatic Zone); iii) the Dent Blanche Nappe and Sesia-Lanzo Zone (Austroalpine units); iv) the Piemontese metaophiolites and remnant-ocean turbidites (Penninic oceanic nappes); v) the Briançonnais Zone, the Internal Penninic massifs, and the Lepontine Dome (Penninic continental nappes); vi) the External massifs with their sedimentary covers (Dauphinois-Helvetic Zone).

The Southern Alps expose a complete lithospheric section of the Adriatic continental margin (Garzanti *et al.*, 2006), including lower crustal gabbros and up to granulite-facies metasediments of the Ivrea-Verbano Zone, amphibolite-facies metasediments of the Variscan basement, Permian volcaniclastics and conglomerates, Triassic carbonates, and Jurassic to Eocene deep-water strata (Gaetani *et al.*, 1998; Muttoni *et al.*, 2005). In close association with the Insubric (Periadriatic) Fault, a major retro-thrust accommodating the dextral transpression between Europe and Adria (Schmid *et al.*, 1989), a series of tonalitic-granodioritic plutons were intruded around 32-30 Ma (von Blanckenburg *et al.*, 1998; Ji *et al.*, 2019). The Austroalpine Sesia-Lanzo Zone contains albite gneisses, eclogitic garnet-micaschists and glaucophanites (Compagnoni *et al.*, 1977), whereas the Dent Blanche Nappe includes granulite-to amphibolite-facies basement rocks, upper Paleozoic metagranitoids, and a thin cover of Mesozoic carbonates with greenschist-facies Alpine overprint (Desmons *et al.*, 1999).

The Penninic continental nappes represent the remnants of the hyper-extended European margin (Manatschal and Bernoulli, 1999) subducted to various depths during the early collisional stage. Blueschist and eclogite-facies metamorphism up to ultrahigh-pressure conditions characterize the Briançonnais basement and the Internal Penninic massifs, respectively (Compagnoni *et al.*, 1995). The Piemontese Zone includes a structurally lower unit of eclogitized ophiolites with greenschist-facies overprint, and an upper unit of calcschists with sparse ophiolite bodies (Lemoine and Tricart, 1986).

In western Liguria, thrust sheets of the Upper Cretaceous turbidites overlying mudrocks locally including ophiolitic slivers display westward-decreasing anchimetamorphic overprint (Di Giulio, 1992). One of these units, deposited in the Piedmont-Ligurian oceanic basin during the Campanian to Maastrichtian, is the >250 m-thick Bordighera Sandstone. This unit, underlain by deep-water mudrocks of the San Bartolomeo Formation, mainly consists of medium-to thick-bedded, medium-grained to gravelly turbidites and is overlain by the San Remo calcareous turbidites (Müller *et al.*, 2017, 2018).

The Internal Penninic massifs consist of amphibolite-facies gneisses and schists intruded by upper Paleozoic granitoids (Dal Piaz and Lombardo, 1986). The Briançonnais Zone includes Variscan basement overlain by the Carboniferous conglomerates with coal lenses, the Permian to Triassic meta-conglomerates, quartzites, carbonates and evaporites, and the Jurassic-Palaeocene pelagic sediments (Lemoine *et al.*, 1986; Desmons, 1992).

The External massifs are inverted listric wedges of European basement, including Variscan or older orthogneisses, migmatites, and amphibolite-facies metasediments, intruded by granites (von Raumer *et al.*, 1999). Their sedimentary cover, including the Permian clastic rocks and Mesozoic carbonates overlain by Eocene nummulitic limestones and turbidites, displays mostly very-low-grade Alpine overprint (Oberhänsli *et al.*, 2004). The Alpine fold-thrust belt is flanked to the north by the Swiss molasse basin, where Alpine detritus accumulated throughout the Oligo-Miocene (Homewood *et al.*, 1986; Schlunegger *et al.*, 1997), and to the west by a series of basins (Dumont *et al.*, 2012), the stratigraphy of which is described below.

2.2. Stratigraphy of the study area

Scaglia-facies marly limestones are widely distributed in the Annot-Peira Cava areas in the French Alps. These pelagic strata, dated as Late Cretaceous by planktonic foraminifera (Ravenne *et al.*, 1987), are truncated by a regional angular unconformity generally interpreted as related to the onset of continental collision and consequent transition from passive-margin to foreland-basin sedimentation in front of the nascent Alpine orogen (Gupta and Allen, 2000). This unconformity was modelled as having been caused by flexural uplift of a forebulge above sea level in response to thrust loads (Jordan and Flemings, 1991; Allen *et al.*, 1991; Crampton and Allen, 1995).

Between the Eocene and the Miocene, different sedimentary basins with distinct depocenters developed along the western front of the French Alps. In the Annot-Peira Cava area, the Cretaceous pelagic limestones were unconformably overlain (Fig. 3B and C) by alluvial conglomerates (“*Infranummulitique*”, Poudingues d'Argens, or Microcodium Formation) (Fig. 3D and E), followed by nummulitic limestones (Calcaires à Nummulites), offshore *Globigerina* marls (Marnes Bleues), and turbiditic sandstones (Grès d’ Annot; Ravenne *et al.*, 1987; Callec, 2004) (Fig. 3F and G; Fig. 4).

Numerous biostratigraphic studies on these three units reported rich, age-diagnostic fossiliferous assemblages including planktonic and larger benthic foraminifera, and calcareous nannofossils (Martini, 1971; Campredon, 1977; Sztrákos and du Fornel, 2003; Callec, 2004; du Fornel *et al.*, 2004). Paleogene sedimentation in the Alpes Maritimes and Alpes de Haute Provence regions began with the continental Microcodium Formation overlain by the *Cerithium* layers, the Calcaires Nummulitiques and the Marnes Bleues, overlain in turn by the turbidites of the Grès d’Annot (Sztrákos and du Fornel, 2003). Sedimentation started in the *Nummulites perforatus* Zone (NP) close to the base of the *Truncorotaloides rohri* Zone (P 14), and ended in the *Cassigerinella chipolensis—Pseudohastigerina micra* Zone (P 18) and in the NP21 nannoplankton Zone documented in the upper part of the Grès d’Annot. More biostratigraphic markers allowed a refined local biozonation (biozones AMP 1 to AMP 7; Sztrákos and du Fornel, 2003) and four local zones were additionally defined by the last occurrence of *Nummulites millecaput* and *N. perforatus—N. ptukhiani*, and by the first appearance of *Nummulites retiatus* (AMGF 1—4) (see Fig. 2).

The Middle Eocene-Lower Oligocene deepening-upward succession has been classically interpreted as being deposited in a foreland basin that subsided under the load of the growing Alpine fold-thrust belt (Evans and Elliott, 1999), and thus baptized as the “*underfilled trinity*” by Sinclair (1997). In foreland-basin models, such *underfilled trinity* was considered as the typical basal part of the succession deposited at a time of limited siliciclastic supply from the developing orogen.

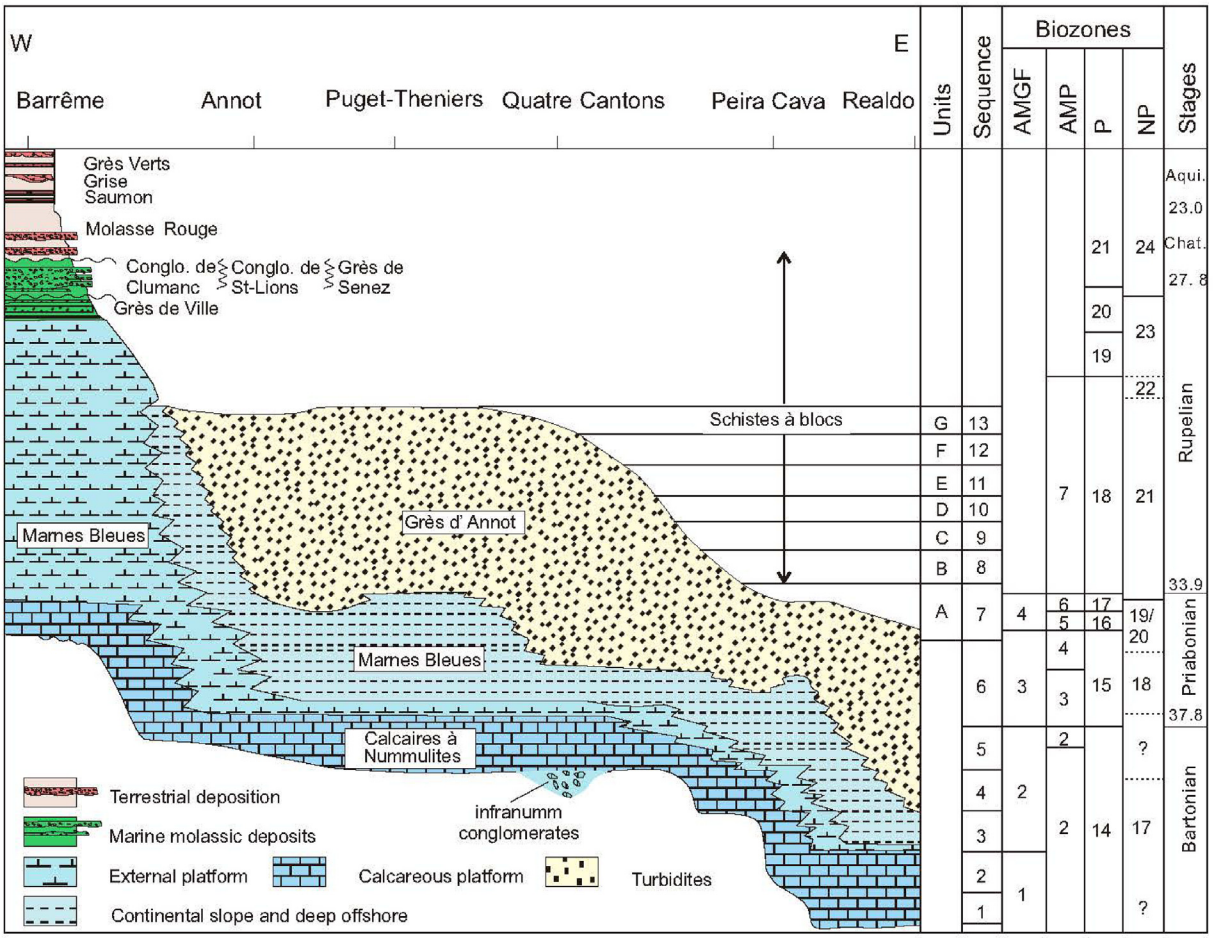

Fig. 2 Lithostratigraphic framework for the Barrême, Annot, Puget-Theniers, Quatre Cantons, Peira Cava, and Realdo sedimentary basins (modified from Sztrákos and du Fornel, 2003). Subdivision of "Units" and "Sequence" for the stratigraphy refers to Sztrákos and du Fornel (2003). Abbreviations: Aqui. = Aquitanian; Chat. = Chattian; infranumm = infranummulites.

In the Late Oligocene, the main depocenter migrated westward to the Barrême Basin (Figs. 1 and 2), where the Marnes Bleues were conformably followed by deltaic sandstones and conglomerates (Grès de Ville, Conglomérats de Clumanc, and the coeval Grès de Senez and Conglomérats de Saint-Lions; Evans and Elliott, 1999). These units were unconformably overlain by coarser fluvial clastic rocks, including the Série des Grès Verts at the top, and collectively termed "molasse" (Joseph *et al.*, 2012).

In the Barrême Basin, the Grès de Ville was assigned to the Early Oligocene P20 planktonic foraminiferal zone (~30 Ma; Callec, 2001). Sole marks and current ripples indicate NNE/NNW-directed paleocurrents (Stanley, 1961). The overlying succession varies notably from north to south. Biostratigraphic data constrain the Conglomérats de Clumanc in the north as late Rupelian in age (P20 and P21 planktonic foraminiferal and NP24 nannoplankton zone). The unit, containing indicators of westward palaeocurrents, displays a progressive upward increase of orogenic detritus, long considered as derived from internal Alpine units (Gubler, 1958), and of andesitic detritus, considered as supplied by the Saint-Antonin volcanism dated between 31.0 Ma (Féraud *et al.*, 1995) and 29.4 Ma (Montenat *et al.*, 1999). The Conglomérats de St-Lions, deposited in the middle of the Barrême Basin, indicate southward paleoflow (De Graciansky *et al.*, 1982; Evans and Elliott, 1999) and contain pebbles suggesting provenance from internal Alpine units (Bodelle, 1971; Evans and Mange-Rajetzky, 1991). In the south, the Grès de Senez are interpreted as northward-prograding shoreface deposits. This marine unit is unconformably overlain by a continental succession including the Molasse Rouge, the Série Saumon, the Série Grise, assigned to the late Chattian (latest Oligocene), and finally by the fluvial Série des Grès Verts containing ultramafic rock fragments (Graciansky *et al.*, 1971). The Barrême Basin is generally interpreted as an overfilled piggy-back basin developed in the Early Oligocene, when the Grès

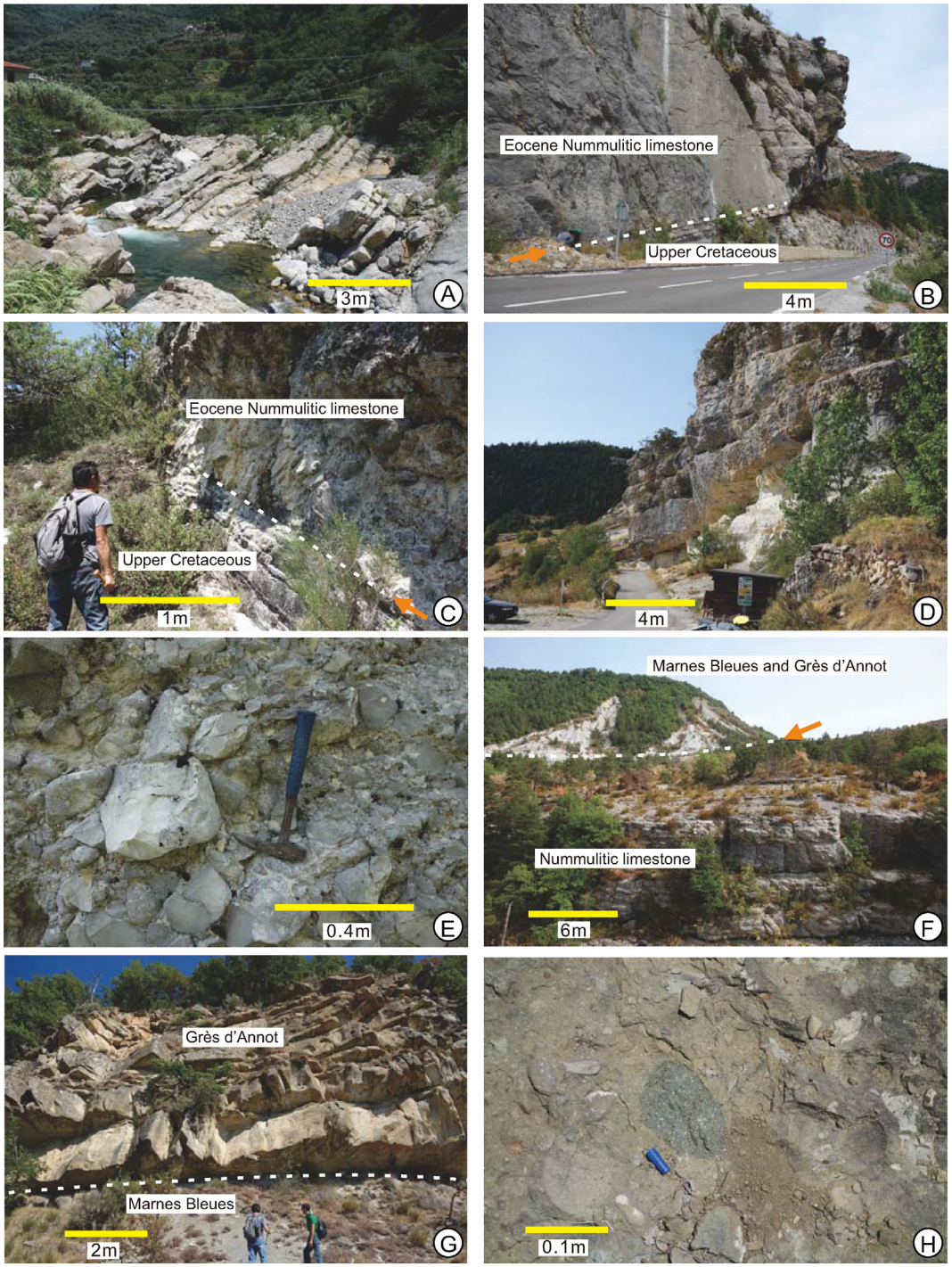

Fig. 3 Field photographs. **A)** Turbiditic sandstones in the Upper Cretaceous Bordighera Formation near Badalucco (GPS N43°54′32.43, E7°50′37.83); **B)** Eocene Nummulitic limestone resting unconformably on Upper Cretaceous pelagic limestones near Les Scaffarels, south of Annot; **C)** Contact between uppermost Cretaceous pelagic limestones and Eocene Calcaires à Nummulites (D73 section, Peira Cava) marked by a decimetric conglomerate layer at the base of Calcaires à Nummulites; **D)** Poudingues d'Argens channelized conglomerates near Peyresq; **E)** Close-up view of Poudingues d'Argens conglomerates near Gion (Barrême Basin); **F)** Eocene Calcaires à Nummulites overlain by *Globigerina* marls (Marnes Bleues), and Grès d'Annot turbiditic sandstones along D101 road near Draux; **G)** Sharp contact between *Globigerina* marls and Grès d'Annot at St. Benoit; **H)** Clumanc conglomerates with an andesitic pebble near Clumanc.

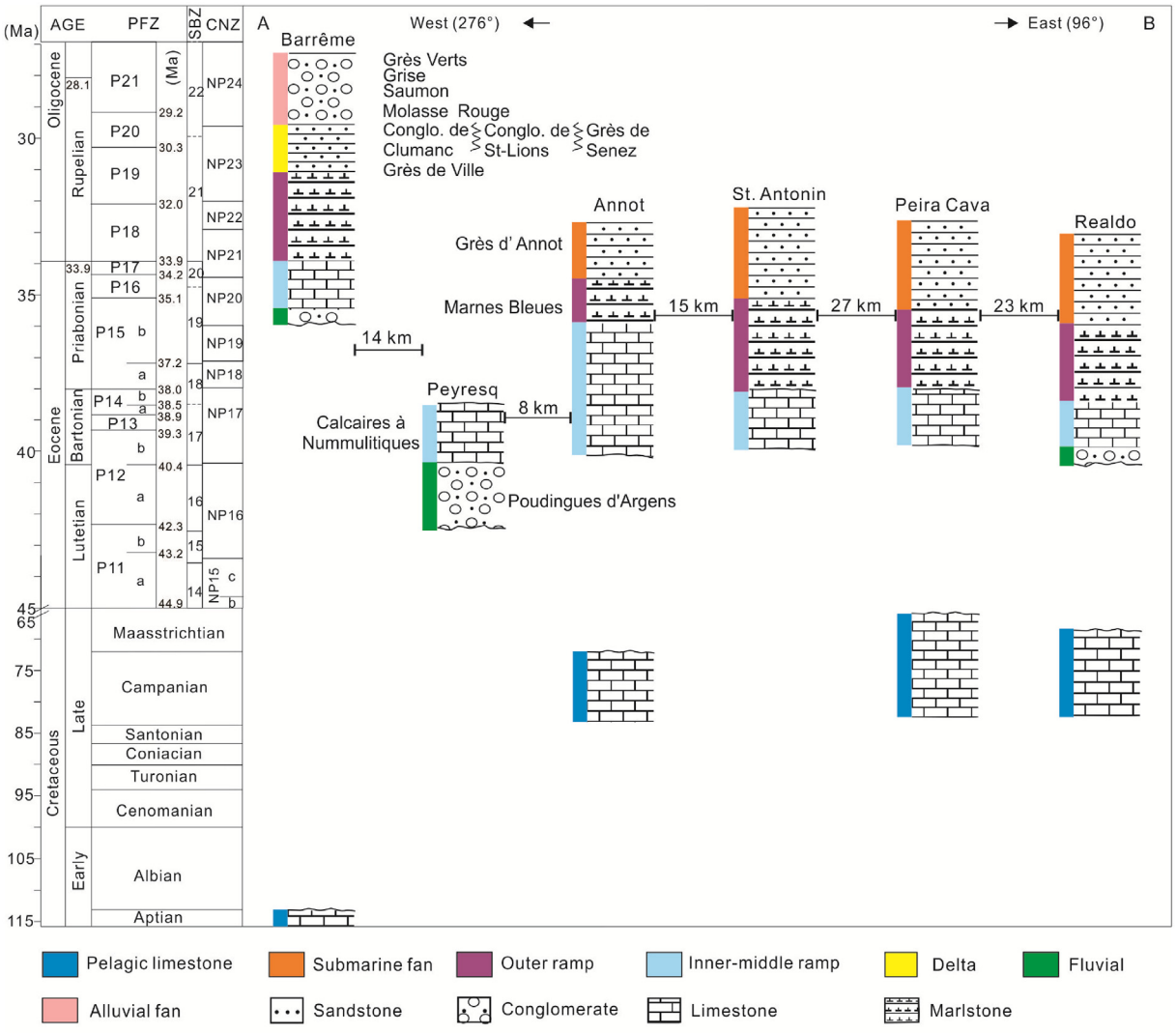

Fig. 4 Ages of lithostratigraphic units in the studied Barrême, Peyresq, Annot, St. Antonin, Peira Cava, and Realdo sedimentary sections, updated with new data from Sztrakos and du Fornel (2003). Lithology and sedimentary facies are indicated for each unit. Age data refer to Figs. S2-1 to S2-5. PFZ = planktonic foraminiferal zone; CNZ = calcareous nannofossil zone; SBZ = larger benthic foraminiferal zone. Section locations (from A to B) are found in Fig. 1.

d'Annot was already accreted to the fold-thrust belt (Joseph *et al.*, 2012).

3. Methods

3.1. Sampling

The studied Upper Cretaceous to Cenozoic sedimentary successions of the Western Alps are exposed in the Annot, Barrême, St. Antonin, and Peira Cava basins in SE France, and in the Realdo and Badalucco basins in NW Italy (Fig. 1). Six stratigraphic sections of the Calcaires à Nummulites were logged and systematically sampled for biostratigraphic and microfacies analysis, including the Sauzeries section in the Barrême Basin (16 samples), the Peyresq section (9 samples) and the Coulomp River section (50 samples) in the Annot Basin, the La Rochette section in the St. Antonin Basin (5 samples), the D73 section in the Peira Cava Basin (37 samples), and the Realdo section in the Realdo Basin (>40 samples). Siliciclastic rocks sampled for provenance analysis include the Upper Cretaceous Bordighera Formation Sandstone (Fig. 3A) in the Badalucco Basin, the Grès d'Annot in the Annot, St. Antonin and Peira Cava basins, and the Grès de Ville, Conglomérats de Clumanc, Grès de Senez, Conglomérats de Saint-Lions, and Sèrie des Grès Verts in the Barrême Basin. Information on measured stratigraphic sections and sampling localities with GPS positions are given in Appendixes Table S1.

3.2. Biostratigraphy and carbonate microfacies

Larger benthic foraminifera (LBF) were determined based on their characteristically complicated endoskeleton (BouDagher-Fadel, 2018) from more than 150 randomly thin-sectioned samples. Planktonic foraminiferal (PF) biostratigraphy in thin section was based on the zonation of BouDagher-Fadel (2015), correlated with the LBF zones (Shallow Benthic Zonation, SBZ) for the Paleogene of the Western Tethys (Serra-Kiel *et al.*, 1998, 2020) and calibrated according to the chronostratigraphic chart of Cohen *et al.* (2013).

Carbonate and mixed siliciclastic—carbonate rocks were classified based on Dunham (1962), Embry and Klovan (1971), and Mount (1985). Microfacies analysis was based on both outcrop and thin-section observations of sedimentary structures, textures, mineralogy, and faunal and floral assemblages. Gastropods, mollusks, echinoderms, large, small and agglutinated benthic foraminifera, and calcareous red and green algae were identified according to descriptions in Flügel (2010). Environmental interpretations were made following Wilson (1975) and Flügel (2010).

3.3. Sandstone petrography and heavy minerals

Thirty-one sandstone samples showing minor diagenetic alteration (5 from Upper Cretaceous Bordighera Formation, 18 from Upper Eocene-Lower Oligocene Annot Formation mainly from St. Benoit, Braux, and Annot sections; 8 Lower Oligocene to Miocene sandstones including Grès de Ville, Grès de Senez, Conglomérats de Clumanc, Conglomérats de St-Lions, and Grès Verts from the Barrême Basin) were selected for modal analysis (Fig. 3). At least 400 grains were identified and counted in each sample following the Gazzi-Dickinson method, in which crystals or grains occurring within rock fragments and larger than ~62.5 μm are counted as single minerals (Ingersoll *et al.*, 1984). Sandstones were classified according to the three main groups of framework components (Q = quartz; F = feldspars; L = lithic fragments), considered where exceeding 10% QFL and listed in order of abundance (classification scheme after Garzanti, 2019b). A feldspatho-quartzose sandstone is thus defined as Q > F > 10% QFL > L, formally distinguishing between feldspar-rich (Q/F < 2; K-feldspar-rich if K-feldspar/plagioclase >2, plagioclase-rich if plagioclase/K-feldspar >2) and quartz-rich (Q/F > 4) compositions. Results of petrographic analysis are provided in Appendix Table 2.

Seven samples from the Grès d'Annot were selected for heavy-mineral analysis. After gentle hand crushing of sandstone samples in an agate mortar, from the wide 32—500 μm size class obtained by wet sieving heavy minerals were separated by centrifuging in Na-polytungstate (2.90 g/cm^3) and recovered by partial freezing with liquid nitrogen. In grain mounts, ≥200 transparent heavy minerals for each sample were either grain counted by the area method or point-counted at an appropriate regular spacing to obtain correct volume percentages. Dubious grains were checked by Raman spectroscopy (Andò and Garzanti, 2014). To characterize heavy-mineral suites, we used the tHMC index (weight percentage of transparent dense minerals of detrital extrabasinal origin; Garzanti and Andò, 2019) and the ZTR index (sum of zircon, tourmaline and rutile; Hubert, 1962).

3.4. Detrital-zircon U—Pb dating

Twelve sandstone samples were selected for U—Pb geochronological analysis. Samples were crushed and dense minerals were separated by elutriation and magnetic methods. Zircon grains were hand-picked, mounted in epoxy resin, and polished. U—Pb dating was conducted by ICP-MS using Agilent 7500a at the State Key Laboratory of Mineral Deposits Research (MiDeR, Nanjing University) and Agilent 7700x at the Laboratory of Earth Surface Process and Environment (LESPE, Nanjing University). Both instruments were equipped with a GeoLas Pro 193 nm laser sampler. At MiDeR, a laser beam with 32 μm diameter was operated at 5 Hz and 8 J/cm^2 fluence. We used zircon standard GEMOC GJ-1 (Jackson *et al.*, 2004) for isotopic fractionation correction, and zircon standard Mud Tank (Black and Gulson, 1978) to monitor instrumental reproducibility and stability, obtaining $^{206}Pb/^{238}U$ ages of 600 ± 9 Ma (n = 224) and 752 ± 22 Ma (n = 56), respectively. At LESPE, a laser beam with 25 μm diameter was operated at 10 Hz and 2—3 J/cm^2 fluence. We used Zircon 91500 to calibrate isotopic fractionation and GJ-1 zircon (Jackson *et al.*, 2004) for accuracy monitoring, obtaining $^{206}Pb/^{238}U$ ages of 1056 ± 58 Ma (n = 209) and 599 ± 4 Ma (n = 70), respectively.

The software GLITTER (version 4.4) was used to calculate raw data (www.mq.edu.au/GEMOC); analytical uncertainties were expressed as 1σ. Common Pb was corrected following Andersen (2002). Isoplot 4 software (Ludwig, 2012) was used to plot probability-density curves and calculate weighted mean ages. $^{206}Pb/^{238}U$ zircon ages were preferred for grains <1000 Ma and $^{207}Pb/^{206}Pb$ ages for grains >1000 Ma. Zircons with discordance >10% were

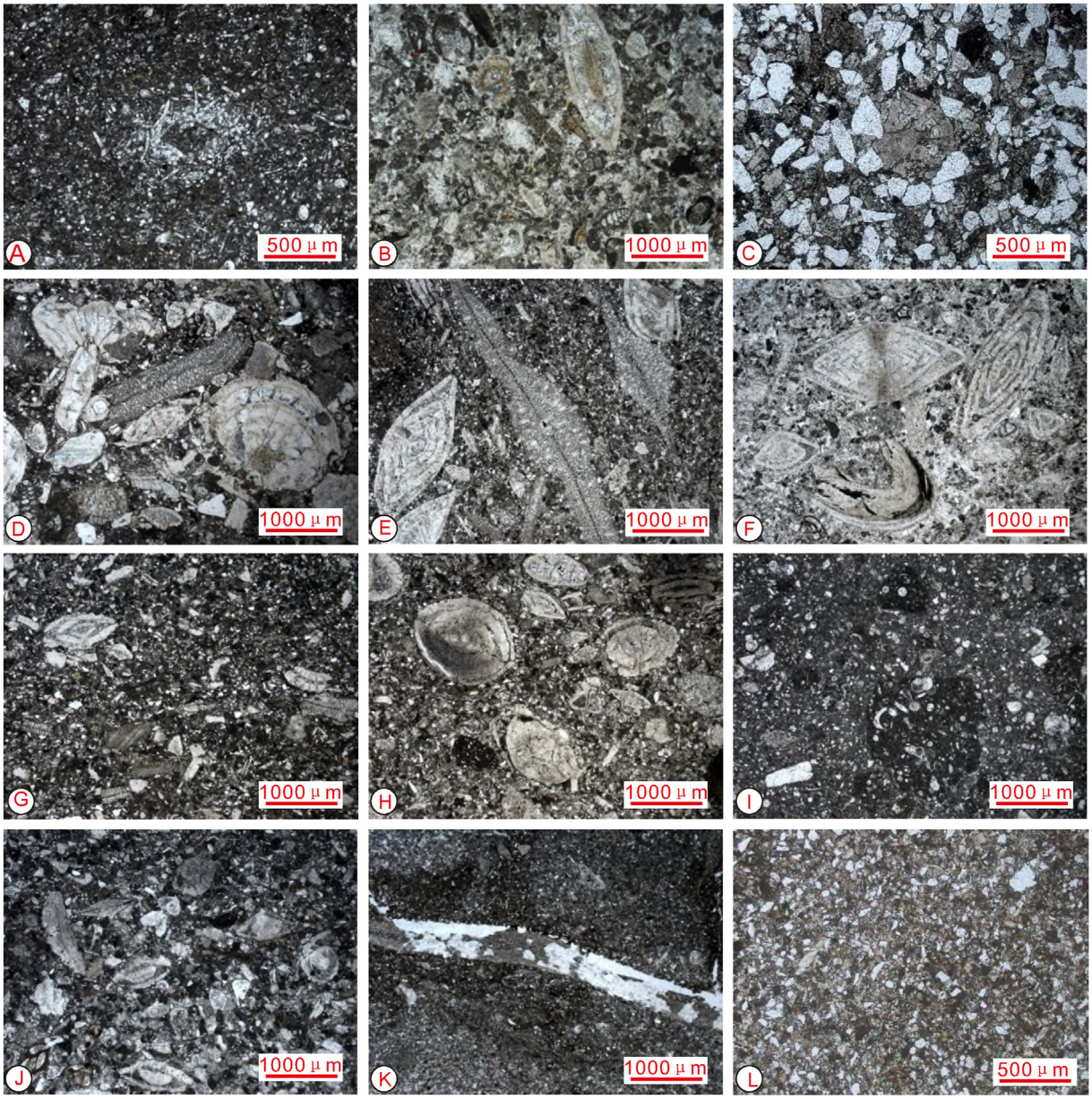

Fig. 5 Identified microfacies (MF1 to MF8). **Upper Cretaceous**: **A)** spiculite and planktonic foraminiferal wackestone/packstone (MF1). **Calcaires à Nummulites**: **B)** bioclastic packstone/rudstone (MF2); **C)** micritic bioclastic sandstone (MF3); **D)** large *Nummulites* rudstone (MF4b); **E)** large *Nummulites* wackestone (MF4a); **F)** poorly-sorted large *Nummulites* grainstone (MF4c); **G)** bioclastic packstone (MF4d); **H)** small *Nummulites* wackestone (MF5); **I)** wackestone with intraclasts and small bioclasts (MF6). **Calcaires à Nummulites and Marnes Bleues**: **J)** bioclastic packstone (MF7a); **K)** *Asterocyclina* wackestone (MF7b); **L)** very fine-grained sandy bioclastic packstone with glaucony (MF8).

excluded in data presentation and interpretation. The complete dataset is provided in dataset Table S2—S5.

4. Cretaceous-Eocene foraminiferal biostratigraphy

The detailed distribution and ages of foraminifera from the topmost Cretaceous pelagic limestones and Calcaires à Nummulites in the Sauzeries (Fig. S2-1; Barrême Basin, see Fig. 6), Peyresq (Fig. S2-2; Annot Basin), Coulomp River (Fig. S2-3; Annot Basin), La Rochette (Fig. S2-4; St. Antonin Basin), and D73 stratigraphic sections (Fig. S2-5; Peira Cava Basin) are provided as Supplementary Material.

4.1. Top of Cretaceous pelagic limestones

Foraminiferal assemblages from the top of the pelagic limestones in the Realdo section include

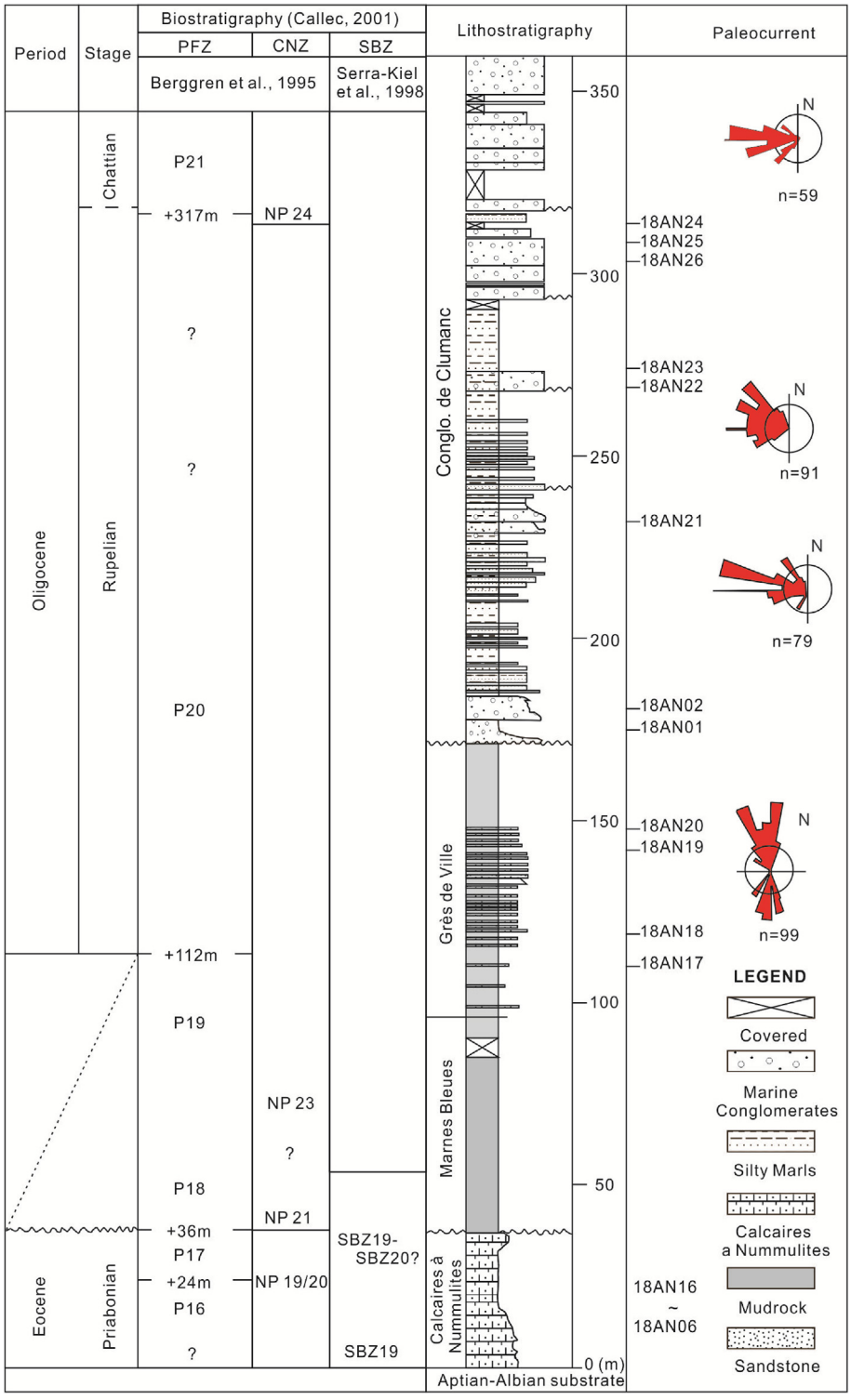

Fig. 6 Stratigraphic section measured in the Sauzeries ravine (Barrême Basin) extending from the Calcaires à Nummulites to the Conglomérates de Clumanc (modified from Joseph *et al.*, 2012). Lithostratigraphic subdivisions and position of studied samples are shown. Paleocurrent directions from Joseph *et al.* (2012). PFZ, CNZ, and SBZ = planktonic-foraminifera, calcareous-nannofossil, and shallow-benthic-foraminifera zones.

Alanlordella subcarinata, Abathomphalus mayaroenis (Fig. S1-1, 1), *Globigerinita conica* (Fig. S1-1, 2), *Pseudotextularia elegans*, and *Globotruncanita stuarti*, pointing to a Maastrichtian 2—3 age.

In the Coulomp River section, the topmost pelagic limestones contain *Globotruncana aegyptiaca, G. bulloides* (Fig. S1-1, 6), *Hedbergella holmdelensis, Heterohelix globulosa, H. reussi, Rugoglobigerina macrocephala* (Fig. S1-1, 8), *R. rugosa*, and *Rugotruncana subcircumnodifer* (Fig. S1-1, 7), pointing to a Campanian 3 age.

In the D73 section, *G. aegyptiaca* (Fig. S1-1, 5), *G. hilli* (dataset Fig. S1-1, 3), *G. linneiana* (dataset Fig. S1-1, 4), *Hedbergella monmouthensis, R. macrocephala*, and *R. rugosa* indicate a Campanian 3-Maastrichtian age.

4.2. Calcaires à nummulites

In every basin from SE France to NW Italy, Upper Cretaceous pelagic limestones and Eocene strata are separated by a major unconformity incised into different levels of the underlying succession, at places removing more than 300 m of strata (Apps *et al.*, 2004). In the Sauzeries section (Fig. 6), the Calcaires à Nummulites unconformably overlie the Lower Cretaceous (Aptian-Albian) marls. In the Annot, Peira Cava, and Realdo sections, mildly deformed Cretaceous limestones are abruptly overlain by the Calcaires à Nummulites (Fig. 3B and C). Whereas, in the Argens, Peyresq, Melina, Sausses, Quatre Cantons, Entrevax, St. Antonin, and Barrême areas, the unconformity is overlain by the Poudingues d'Argens, followed by the Calcaires à Nummulites (Apps *et al.*, 2004) (Fig. 3D and E).

In the Barrême Basin, the 15-20 m-thick Calcaires à Nummulites conformably overlie the Poudingues d'Argens and contain *Chiloguembelina woodi, Globorotalia nana, Heterostegina gracilis, Nummulites aturicus, Nummulites bullatus, Nummulites fabianii, Operculina* ex. gr. *gomezi, Spiroclypeus carpaticus*, and *Turborotalia centralis*. These Larger Benthic Foraminifera (LBF) indicate a late Priabonian (SBZ19) age, confirming the results of Bodelle (1971) (Fig. S2-1).

In both Annot (dataset Fig. S2-2; S2-3, S2-4) and Peira Cava areas (Fig. S2-5), LBF assemblages are dominated by *Nummulites* and *Discocyclina* (Fig. S1-2), documenting zones from SBZ17 to SBZ19. The first appearance of *Nummulites perforatus* (Fig. S1-2, 1) indicates the earliest Bartonian (SBZ17, P12b-P14, 41.2—38 Ma). Assemblages dominated by *Discocyclina dispansa* (Fig. S1-2, 2), *Fabiania cassis* (Fig. S1-2, 3), *Operculina* ex. gr. *gomezi* (Fig. S1-2, 4), and *Nummulites incrassatus* (Fig. S1-2, 5) point to the early Bartonian age. The first appearance of *Nummulites biedai* (Fig. S1-2, 6) with *Pellatispira* sp. (Fig. S1-2, 7a) and still common *O.* ex. gr. *gomezi* and *N. incrassatus* indicate the base of the late Bartonian age. The planktonic foraminifera *Hantkenina alabamensis* (Fig. S1-1, 9), *Turborotalia cerroazulensis* (Fig. S1-1, 10), *Globigerina praebulloides* (Fig. S1-1, 11), *Catapsydrax dissimilis* (Fig. S1-1, 12), *Globigerinatheka* sp. (Fig. S1-1, 13), *Dentoglobigerina pseudovenezuelana* (Fig. S1-1, 14), *Globigerinatheka barri* (Fig. S1-1, 15), and *Acarinina* sp. (Fig. S1-1, 16) characterize the latest Bartonian to earliest Priabonian, (P14 — P15, 39.2—35.1 Ma). The Priabonian is defined by the first appearance of *H. gracilis* (Fig.S1-2, 8), associated with *N. fabianii* (Fig. S1-2, 9), *Operculina* sp. A, *N. aturicus* (Fig. S1-2, 10), *Nummulites garnieri*, *Amphistegina* sp., *Heterostegina* spp., *Nummulites ptukhiani*, *Pellatispira* sp., and *Asterocyclina alticostata danubica* (Fig. S1-2, 11). Zones SBZ19/P15 are thus indicated for the top of the Calcaires à Nummulites (~36-35 Ma).

In the Realdo section, the transgressive base of the Calcaires à Nummulites has been dated as later than the base of zone P14/P13 (Sztrákos and du Fornel, 2003), i.e., as not older than 40.5 Ma. Early to middle Bartonian assemblages (SBZ17), identified based on the presence of *Assilina* and lack of *Chapmanina gassinenesis*, characterize most of the unit in the Realdo section. The first occurrence of *Chapmanina gassinensis*, marking the base of SBZ18 (~38 Ma; latest Bartonian), occurs close to the top of the Calcaires à Nummulites (Coletti *et al.*, 2021). The base of the overlying *Globigerina* marls documents a deepening event dated by planktonic foraminifera as comprised between the late Bartonian and the early Priabonian (Varrone and d'Atri, 2007).

Based on these detailed biostratigraphic data, we have revised the former stratigraphic framework. The revised stratigraphy demonstrates no major diachroneity across the western Alpine foreland basins (Fig. 4).

5. Sedimentary facies and microfacies

Eight microfacies (MF1-MF8; Fig. 5) – one characteristic of the uppermost Cretaceous pelagic strata (MF1) and seven corresponding to the Eocene inner-ramp, middle ramp, and outer-ramp environments (MF2 to MF8; Table 1) – were identified by integrating sedimentological and paleontological observations and are described in this Section 5. The sedimentary evolution based on microfacies analysis is discussed in Section 6.

5.1. Late Cretaceous pelagic environment

5.1.1. MF1 spiculite and planktonic foraminiferal wackestone and packstone

In both Annot and Barrême basins, the Upper Cretaceous grey marls and marly limestones, unconformably overlain by the Calcaires à Nummulites, contain common sponge spicules and minor planktonic foraminifera or echinoderm fragments set in a micritic matrix (Fig. 5A). Because of extensive burrowing, microfossils are either scattered or densely packed (Fig. 5A). A micritic matrix with abundant pelagic microfossils associated with shell concentrations indicates a pelagic environment (Flügel, 2010).

5.2. Eocene paleovalley fill

The Poudingues d'Argens consist of moderately to well-sorted channelized conglomerate and breccia intercalated with fine sand, silt, or clay locally containing freshwater gastropods. Rarely imbricated pebbles and cobbles are mostly derived locally from Scaglia-like Cretaceous limestones (Gubler, 1958). In the Barrême and Peyresq areas, clast-supported channelized conglomerates are dominant, with few sandstone intercalations. Channels are a few meters wide, locally display groove casts at the base, and were filled by distinct episodes of high-energy deposition, such as flash floods and sheet flows separated by erosive reactivation surfaces (Apps *et al.*, 2004; Grosjean *et al.*, 2012). This unit is interpreted as representing a paleovalley fill incised during a major tectonically driven drop of base-level (Van Wagoner *et al.*, 2012; Blum *et al.*, 2013).

5.3. Inner ramp

5.3.1. MF2 bioclastic packstone/grainstone

Grey bioclastic packstones occur at the base of the Coulomp River section (Annot Basin). Abundant bioclasts set in micritic matrix (Fig. 5B) include LBF (*Nummulites*, *Sphaerogypsina*, *Chapmanina*, *Eorupertia*, encrusting acervulinids), small miliolids, coralline algae, and some echinoderm fragments and serpulids, together with rare intraclasts and ooids. Larger benthic foraminifera with thick shells and calcareous red algae are typical of the photic zone and platform-margin settings and, together with the lack of common orthophragminids, indicate an inner-ramp to middle-ramp transition close to fair-weather wave base (Beavington-Penney and Racey, 2004; BouDagher-Fadel, 2018).

5.3.2. MF3 micritic sandstone/sandy bioclastic wackestone

In the lower part of the Calcaires à Nummulites exposed in the Barrême Basin, dark grey micritic limestones contain quartz-rich silt to medium sand associated with poorly sorted bioclasts (mainly larger benthic foraminifera) (Fig. 5C). Well-sorted, angular to subangular quartz grains decrease up-section, suggesting a deepening-upward trend. LBF and abundance of angular quartz grains indicate an inner-ramp environment above fair-weather wave base and restricted to open-marine conditions with subordinate siliciclastic supply.

5.4. Middle ramp

5.4.1. MF4 wackestone, grainstone or rudstone with large nummulites

In the middle part of the Coulomp River section, thick-bedded wackestones (MF4b, Fig. 5E) containing *Nummulites*, *Operculina*, *Asterocyclina* and *Discocyclina* are intercalated with rudstone (MF4a, Fig. 5D), grainstone (MF4c, Fig. 5F), and bioclastic packstone commonly displaying erosive base (MF4d, Fig. 5G). Densely packed rudstone and grainstone indicate effective winnowing of micrite. Common erosive bases confirm deposition by turbulent flows in a middle ramp environment frequently affected by storms (Beavington-Penney and Racey, 2004; Flügel, 2010; BouDagher-Fadel, 2018).

5.4.2. MF5 wackestone with small nummulites

In the lower part of the Coulomp River section, thick-bedded grey limestones contain diverse species of small *Nummulites*, associated with coralline algae, other benthic foraminifera, and echinoderm fragments (Fig. 5H). Texture and high diversity of nummulitids point to middle ramp environments, slightly deeper than for MF3 (Beavington-Penney and Racey, 2004).

5.4.3. MF6 wackestone with intraclasts and small bioclasts

At the top of the Calcaires à Nummulites in the Coulomp River section, thick-bedded grey limestones contain abundant planktonic foraminifera, minor small hyaline benthic foraminifera, echinoderms, and reworked micritic intraclasts set in micritic matrix (Fig. 5I). Mixed benthic and planktonic biota, abundant intraclasts, and association with MF4 suggest storm deposition on a middle ramp.

Table 1 Identified microfacies and interpretation of sedimentary environments.

Microfacies		Carbonate grains								Groundmass		Terrigenous grains (percentage, size range)	Sedimentary structures	Standard microfacies (Flügel, 2010)	Depositional environment
		Planktonic foraminifera	Spiculite	Nummulites	Bioclasts	Serpulids	Red algae	Echinoderm	Intraclasts	Matrix	Cement				
MF1	Spiculite and planktonic foraminiferal wackestone and packstone	7	20	—	2			1	—	70	—	—	Bioturbation	RMF1	Pelagic, below SWB
MF2	Bioclastic packstone/ grainstone	—	—	28	3	2	3	3	1	55	5	—	—	RMF26	Inner-ramp to middle-ramp, close to FWWB
MF3	Fine-grained micritic sandstone/sandy bioclastic wackestone	—	—	7	3				—	45	—	45 (0.02—0.25 mm)	—	—	Inner ramp, above FWWB
MF4	Wackestone, grainstone or rudstone with large *Nummulites* (B-forms)	—	—	10—80	10—45	—	—	—	—	20—55	10	—	Erosive surface	RMF14	Middle ramp, episodically influenced by storms
MF5	Wackestone with small *Nummulites* (A-forms)	—	—	35	5				—	60		—	—	RMF13	Middle ramp, episodically influenced by storms
MF6	Wackestone with intraclasts and small bioclasts	—	—	—	5				8	87	—	—		RMF11	Middle ramp, episodically influenced by storms
MF7	*Asterocyclina* wackestone with bioclastic packstone	—	—	7	2	—	—	—	—	91	—	—	—	RMF9	Distal middle ramp or outer ramp, episodically influenced by storms
MF8	Sandy bioclastic packstone	—	—	—	15	—	—	—	—	65	—	20 (0.01—0.03 mm)	—	RMF2	Outer ramp influenced by terrigenous supply

Note: FWWB—fair-weather wave base; SWB—storm wave base.

5.4.4. MF7 Asterocyclina wackestone with bioclastic packstone

At the top of the Calcaires à Nummulites in the Coulomp River section, grey marl interbedded with thin-bedded wackestone comprising 5%—10% scattered *Asterocyclina* (MF7a) (Fig. 5J) are intercalated with bioclastic packstone with *Nummulites*, *Operculina*, *Asterocyclina*, and miliolids (MF7b) (Fig. 5H). Distal middle ramp or outer ramp environments with low-energy background micrite deposition frequently interrupted by storms are indicated (Flügel, 2010).

5.5. Outer ramp

5.5.1. MF8 sandy bioclastic packstone

In the upper part of the Barrême Basin section, dark grey silty marls are interbedded with thin-bedded micritic limestones containing planktonic foraminifera, subordinate small hyaline benthic foraminifera, and sporadic echinoderm fragments and glaucony (Fig. 5L). Glaucony typically grows authigenically on the starved middle shelf at water depths ≥50 m, preferentially during transgression (e.g., Garzanti, 1991). Dominant micrite, terrigenous silt, and lack of lamination reflect weak water turbulence on an outer ramp affected by coastal currents.

6. Sedimentary evolution

The palaeoecology of LBF and carbonate microfacies characterizing the Calcaires à Nummulites allowed us to reconstruct the sedimentary evolution of the Annot and Barrême basins during the Bartonian to Priabonian. The Calcaires à Nummulites unconformably overlie the Upper Cretaceous strata, documenting a change from pelagic to much shallower-water conditions during this more than ~25 myr-long stratigraphic gap, corresponding to the time window when the collision between Europe and Adria began.

6.1. Annot area

The unconformity separating the pelagic Upper Cretaceous strata from the Bartonian base of the Calcaires à Nummulites represents a long stratigraphic gap and a major environmental change (Fig. 7). Spiculite and planktonic foraminiferal packstones/wackestones (MF1) indicate a deep-water depositional environment during the Campanian-Maastrichtian, whereas bioclastic packstones/grainstones (MF2) testify to a much shallower-water middle ramp environment for the Bartonian base of the Calcaires à Nummulites. The overlying succession documents a long-term deepening-upward trend, starting with wackestones with large *Nummulites* (MF4a) interbedded with storm deposits (MF4b, 4c, 4d) and wackestones with small *Nummulites* (MF5) deposited on a middle ramp, passing upward to *Asterocyclina* wackestones (MF7a) intercalated with bioclastic packstones (MF7b) deposited on a deeper-water ramp episodically affected by storms.

6.2. Peira Cava Basin

The Peira Cava Basin displays a similar paleoenvironmental evolution as the Annot area (Fig. 8). Spiculite and planktonic foraminiferal packstones (MF1) deposited in pelagic environments during the Campanian-Maastrichtian are abruptly overlain by micritic sandstone/sandy bioclastic wackestone (MF3) at the base of the Calcaires à Nummulites. The overlying strata document a deepening trend from middle ramp wackestone with large *Nummulites* (MF4a) to sandy bioclastic packstone (MF8) deposited in deeper-water environments affected by siliciclastic supply.

6.3. Realdo section

Two deepening-upward sequences are identified in the Calcaires à Nummulites Formation exposed in the Maritime Alps. The lower sequence begins with a debris-flow deposit with clasts dominantly derived from erosion of the uppermost Cretaceous pelagic marly limestones mixed with shallow-water Eocene bioclasts, overlain by middle ramp limestones containing coralline algae and LBF. Above, wackestones and mudstones with well-preserved planktonic foraminifera are intercalated with packstones rich in reworked shallow-marine bioclasts (mainly LBF and echinoids). Deposition on a proximal outer ramp characterized by downslope transport of inner/middle ramp debris during storms is indicated.

The second sequence starts with an acervulinid foraminifera and coralline algae macroid facies deposited on an inner ramp, as testified by the presence of the large shallow-marine miliolid foraminifera

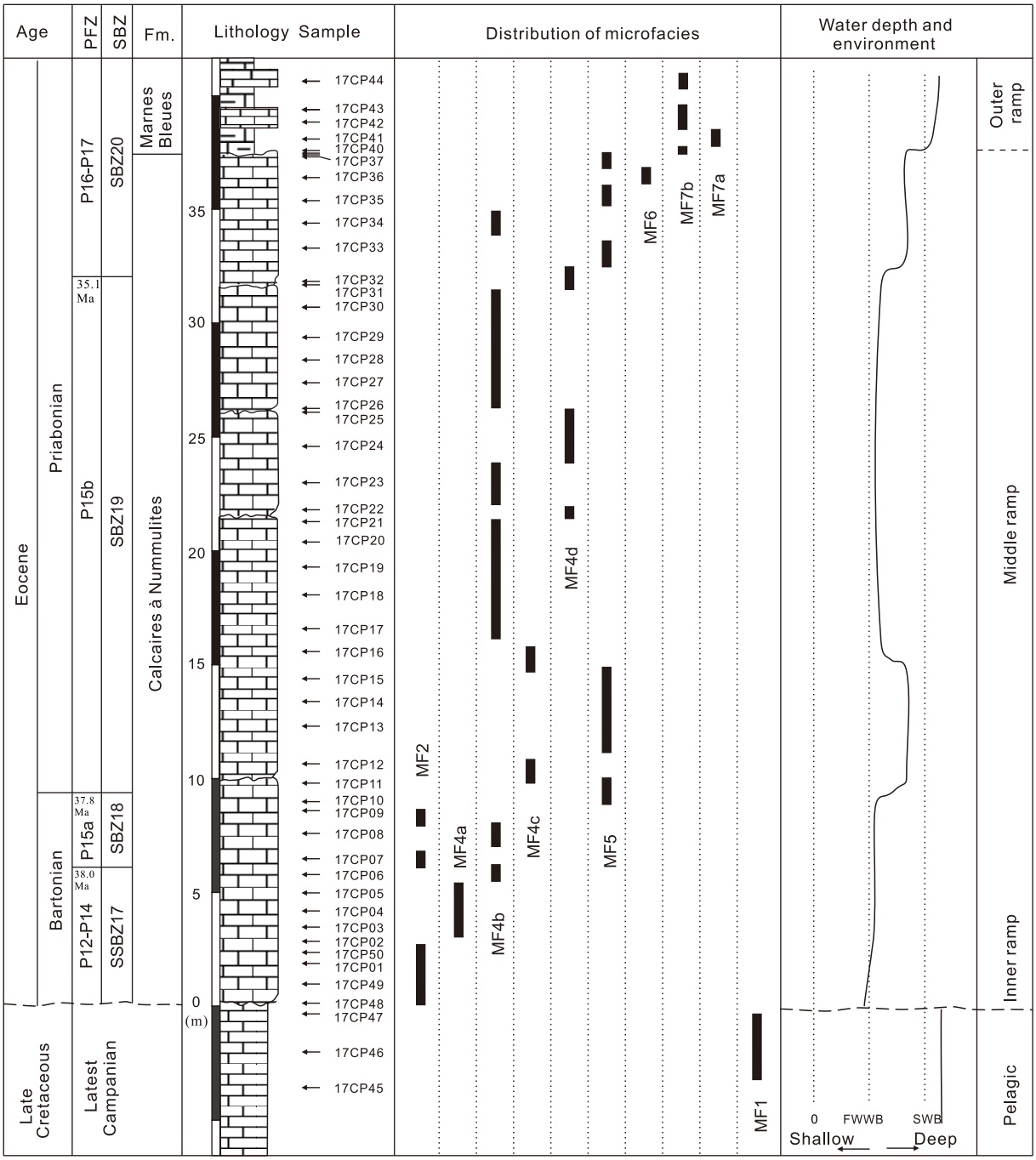

Fig. 7 Lithological log of the Calcaires à Nummulites Formation in the Braux section (Annot Basin). The distribution of carbonate microfacies, interpreted paleowater depths, and sedimentary environments are indicated. Detailed descriptions and interpretations of each microfacies are found in Section 5. PFZ, planktonic foraminiferal zone; SBZ, larger benthic foraminiferal zone.

Alveolina and *Orbitolites*. Above, middle ramp deposits dominated by coralline algae and LBF are followed by proximal outer ramp sediments dominated by discocyclinids. The overlying *Globigerina* marls testify to final deepening.

7. Provenance data and interpretation

The studied samples are listed in dataset Table S1 and their locations are shown in Fig. 1.

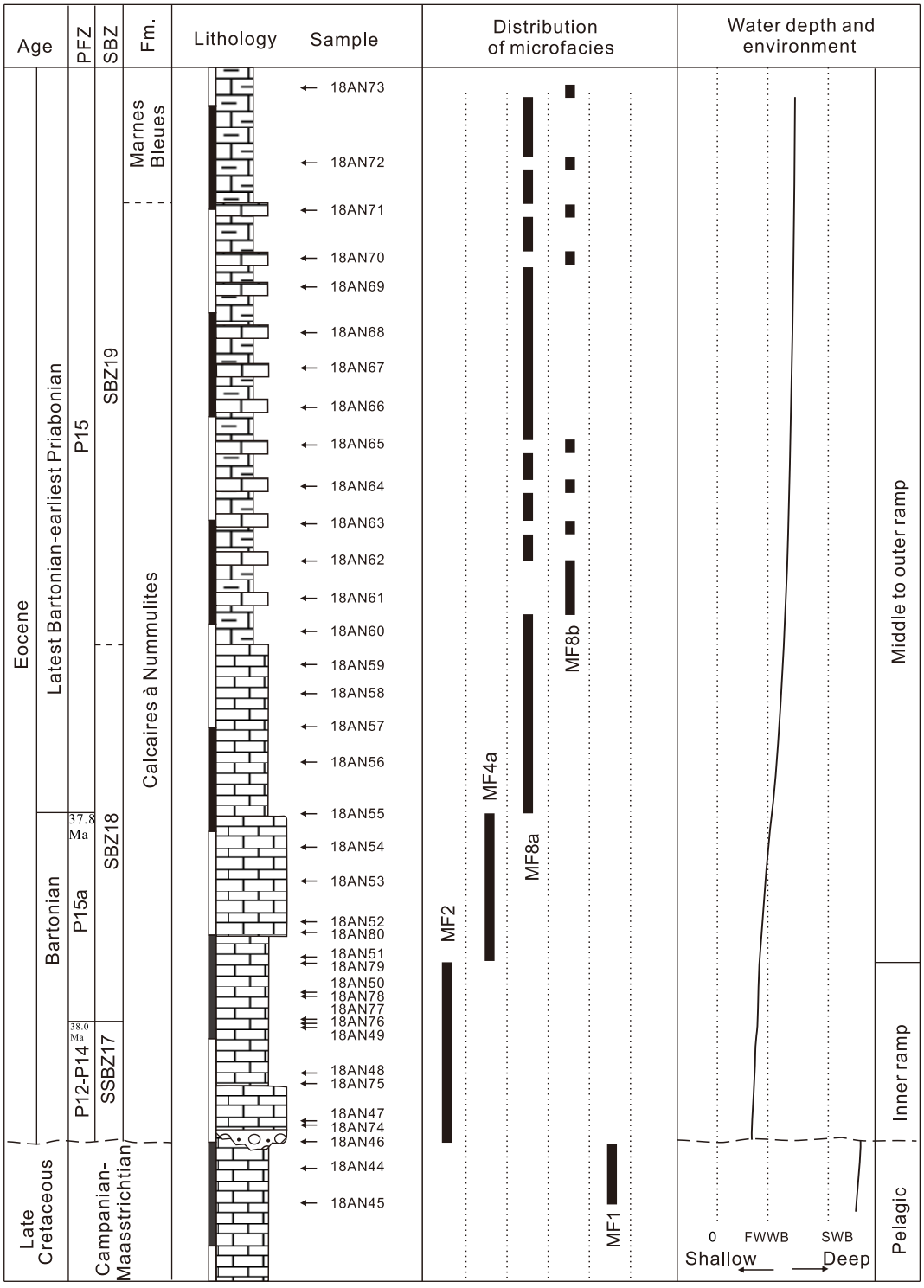

Fig. 8 Lithological log of the Calcaires à Nummulites Formation in D73 section, Peira Cava Basin. The distribution of carbonate microfacies, interpreted paleowater depths, and sedimentary environments are indicated. Detailed descriptions and interpretations of each microfacies are found in Section 5.

7.1. Sandstone detrital modes and heavy minerals

7.1.1. Upper Cretaceous Bordighera turbidites

The Bordighera Sandstone was studied near Badalucco and along the road from Triora to San Bernardo. The four point-counted sandstones are quartzo-feldspathic to K-feldspar-rich feldspatho-quartzose, with mostly monocrystalline quartz (Qp/Q < 1%; P/F < 30%; L/QFL <7%; Fig. 10). Rock fragments are mainly felsic volcanic or granitoid types with subordinate schist (Fig. 9M and N). Our data are consistent with previous results by Müller *et al.* (2018; Fig. 10).

7.1.2. Grès d'Annot

Eighteen samples were analyzed (4 from St. Benoit, 5 from Braux, 4 from Annot, and 5 from four different sites in the Annot area; for a full description of these stratigraphic sections, see Tomasso and Sinclair, 2004). Sandstones range from quartzo-feldspathic to litho-feldspatho-quartzose with mostly monocrystalline quartz (Q/F between 1 and 3; average P/F 37%; average L/QFL 9%; Fig. 10). Rock fragments are mainly felsic volcanic or granitoid types with rare limestone, sandstone, argillite, phyllite, schist, and basalt grains (Fig. 9K and L). The seven samples analyzed for transparent heavy minerals show the same very poor assemblage (tHMC 0.1—0.3), mostly consisting of garnet and apatite, associated with tourmaline, zircon, and minor rutile (ZTR 18—37). Staurolite, epidote, Cr-spinel, sporadic titanite, anatase, monazite, or chloritoid are locally significant.

7.1.3. Oligocene-Miocene sandstones from the Barrême Basin

Five Oligocene-Miocene sandstones from the Barrême Basin are compositionally distinct from the Grès d'Annot. The Grès de Ville (Fig. 9I and J) and the Grès de Senez (Fig. 9C and D) consist of litho-quartzose sandstones with mainly monocrystalline quartz (Q/L between 1 and 8). Most lithics are limestones (>77%) with subordinate felsic volcanic types. Sandstones in the Conglomérats de Clumanc (Fig. 9G) and in the Conglomérats de Saint-Lions (Fig. 9E and F) range from quartzo-litho-feldspathic to quartzo-feldspatho-lithic with mainly monocrystalline quartz and K-feldspar >> plagioclase (Fig. 10). Most lithics are felsic volcanic grains (>86%) with a few limestones and schists. Clasts in the Conglomérats de Saint-Lions are ~60% limestone, ~10% vein quartz, ~10% andesite, ~10% schist, and ~10% purplish-red chert. Clasts in the Conglomérats de Clumanc are mainly limestone associated with andesite, diorite (Fig. 9H), granite, sandstone, and quartzite. The Série des Grès Verts consists of feldspatho-quartzo-lithic sandstones with dominant felsic volcanic and significant ultramafic lithics. The latter are mostly lizardite-bearing cellular serpentine grains (Fig. 9A and B) showing pseudomorphic mesh texture.

Detailed heavy-mineral studies by Evans and Mange-Rajetzky (1991) documented a depleted apatite-staurolite-tourmaline heavy-mineral suite, with minor green augite and green-brown hornblende in the Grès de Ville and occurrence of staurolite, kyanite, andalusite, tourmaline, zircon, and apatite with lack of volcaniclastic detritus in the Grès de Senez. In contrast, volcaniclastic detritus is dominant in the Conglomérats de Saint-Lions, including hastingsitic and basaltic hornblende, euhedral apatite, titanite, and minor augite.

7.2. Detrital zircon geochronology

Detrital zircons from two Cretaceous Bordighera and seven Oligocene Annot sandstones (two each from St. Benoit, Braux and Annot, and one from a sandstone boulder on the riverbed near La Valette, Grand Coyer basin) yielded similar U—Pb age spectra (Fig. 11). Most ages are younger than 700 Ma, clustering at 240—340 Ma (main peak at ~300 Ma), 380—470 Ma, and broadly between 500 and 670 Ma. A few younger ages were obtained (128, 171, 216, and 237 Ma), all notably older than the depositional age. Our geochronological data are consistent with previous results by Chu *et al.* (2016), Müller *et al.* (2018), and Di Giulio *et al.* (2020) (Fig. 11).

Five sandstones from the Barrême Basin show similar zircon-age spectra, but all also yielded a prominent youngest cluster at 29—38 Ma (Fig. 11). Ages of detrital zircons cluster between 380 and 470 Ma in the Grès de Senez and Grès de Ville, and between 240 and 340 Ma in the Conglomérats de Clumanc and in the Conglomérats de Saint-Lions. The Série des Grès Verts is distinguished by a significant 150—180 Ma cluster (peak at ~160 Ma).

7.3. Provenance interpretation

The occurrence of granitoid and felsic volcanic rock fragments, and zircon-age spectra of Grès d'Annot sandstones indicate that they were chiefly derived from granitoid massifs of Variscan and post-Variscan ages, with minor ignimbrite covers, similar to those exposed in diverse Alpine regions, as well as in the Corsica-Sardinia block and the Maures-Estérel Massif of

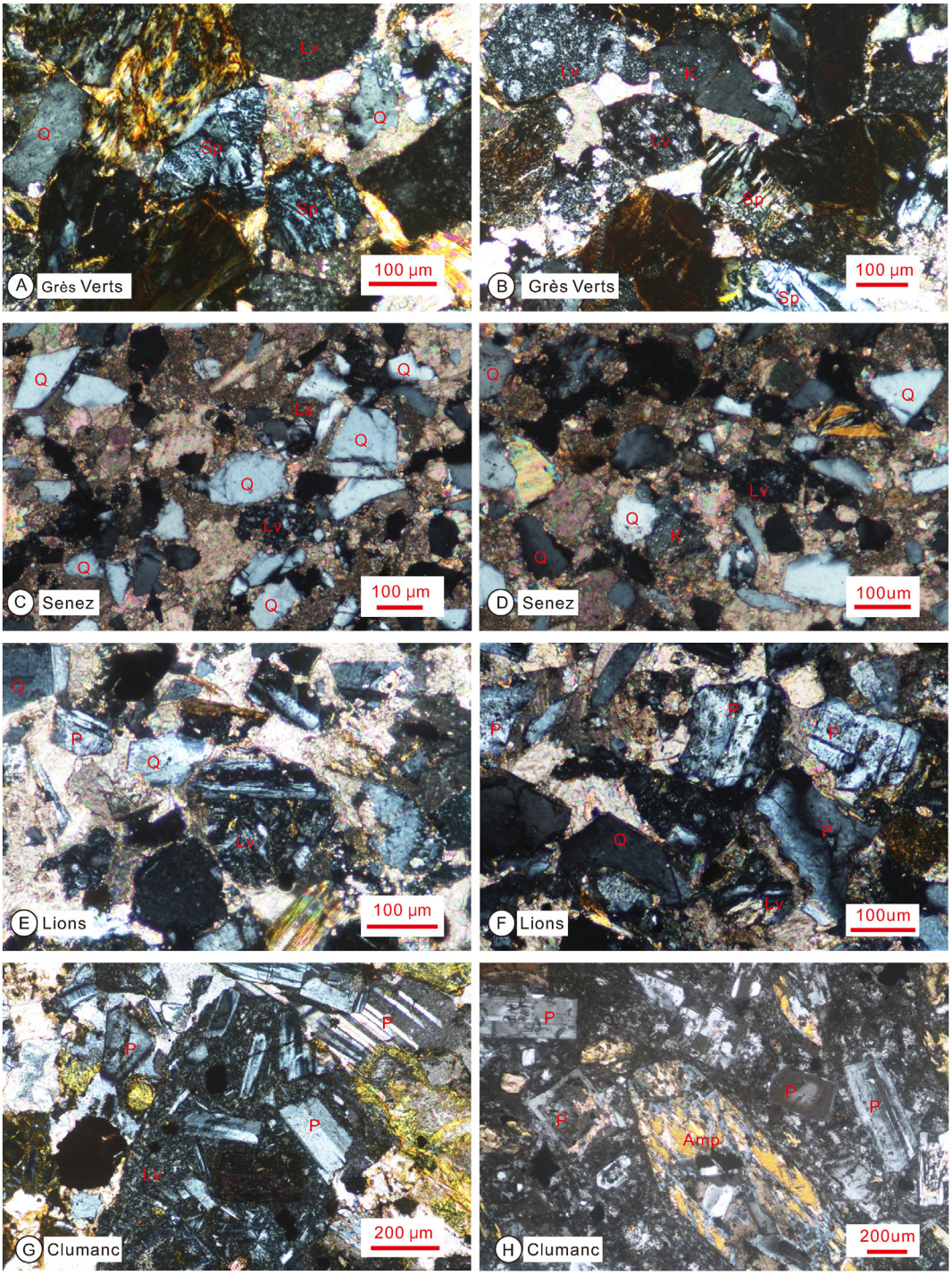

Fig. 9 Microphotographs (taken in cross-polarized light) of the Upper Cretaceous to Oligocene sandstones: **A**) and **B**) feldspatho-quartzo-lithic sandstone (18AN05, Série des Grès Verts); **C** and **D**) litho-quartzose sandstone (18AN04, Grès de Senez); **E** and **F**) quartzo-litho-feldspathic sandstone (18AN29, Conglomérats de Saint-Lions); **G**) quartzo-litho-feldspathic sandstone (18AN22, Conglomérats de Clumanc); **H**) diorite porphyry clast (18AN24-D, Conglomérats de Clumanc); **I** and **J**) litho-feldspatho-quartzose sandstone (18AN17, Grès de Ville); **K**) feldspatho-quartzose sandstone (17AN26, Grès d'Annot); **L**) quartzo-feldspathic sandstone, (17AN10, Grès d'Annot); **M** and **N**) quartzo-feldspathic sandstone (18AN96, Bordighera Sandstone). Q-quartz; P-plagioclase; K-potassium feldspar; Lm-metamorphic lithic, Ls-sedimentary lithic; Lv-volcanic lithic; Sp-serpentinite lithic; Amp-amphibole.

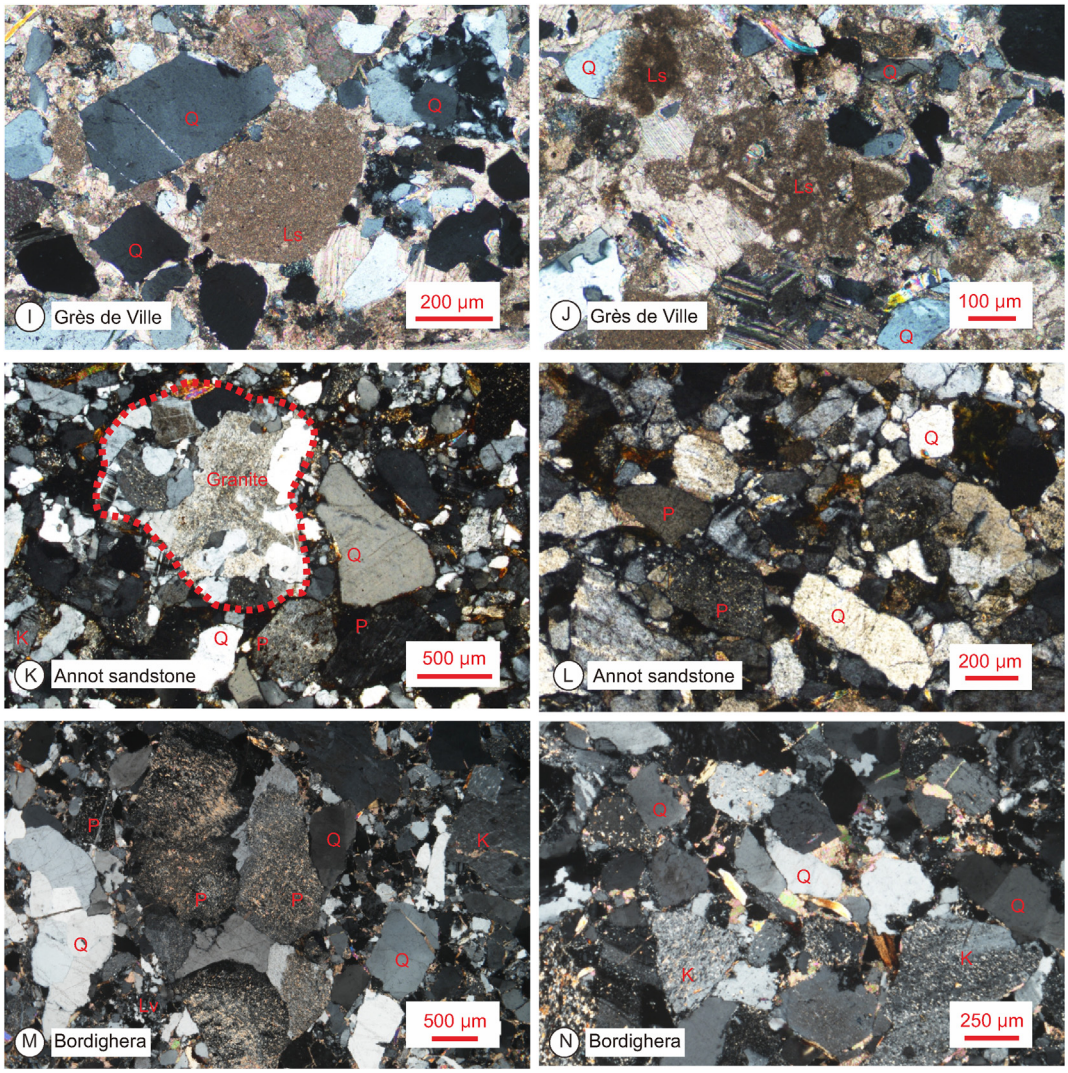

Fig. 9 Continued

southern France. Former paleocurrent studies consistently point to a source located in the south (Joseph and Lomas, 2004; Joseph *et al.*, 2012). The similar detrital modes and zircon-age spectra displayed by the Bordighera Sandstone, now accreted to the Alpine belt, indicates that these remnant-ocean turbidites were fed from a source with similar characteristics as the one that fed the Grès d'Annot.

The heavy-mineral assemblage characterizing the Grès d'Annot is mostly represented by garnet and apatite, associated with zircon, tourmaline, rutile, Cr-spinel, and other relatively durable minerals such as staurolite and chloritoid. The lack of unstable ferromagnesian minerals and the scarcity of epidote indicates severe, but not extreme selective diagenetic dissolution taking place at a depth of a few kilometers during sedimentary or tectonic burial before accretion to the orogenic thrust belt (Morton and Hallsworth, 2007; "*minerofacies 4*" of Garzanti *et al.*, 2018). The presumed loss of unstable species precludes a precise provenance diagnosis. The occurrence of rare Cr-spinel suggests that mantle rocks, mafic lavas, or sediments derived from them were exposed in the source area.

The Bordighera Sandstone was recently interpreted to have been sourced from the down-bending paleo-European plate during impending collision in the Western Alps (Müller *et al.*, 2018, 2019; Di Giulio *et al.*, 2020). We fully concur that detritus was derived from foreland areas rather than from the growing Alpine thrust belt, which is at odds with the classical model of a flexural foreland basin fed from the adjacent orogen. However, we underscore that a flexural bulge would be associated with minor relief and thus represents an unlikely source of abundant detritus. If in the Eocene, the Alpine orogen was not yet developed enough to represent a major source of sediment (e.g., Malusà

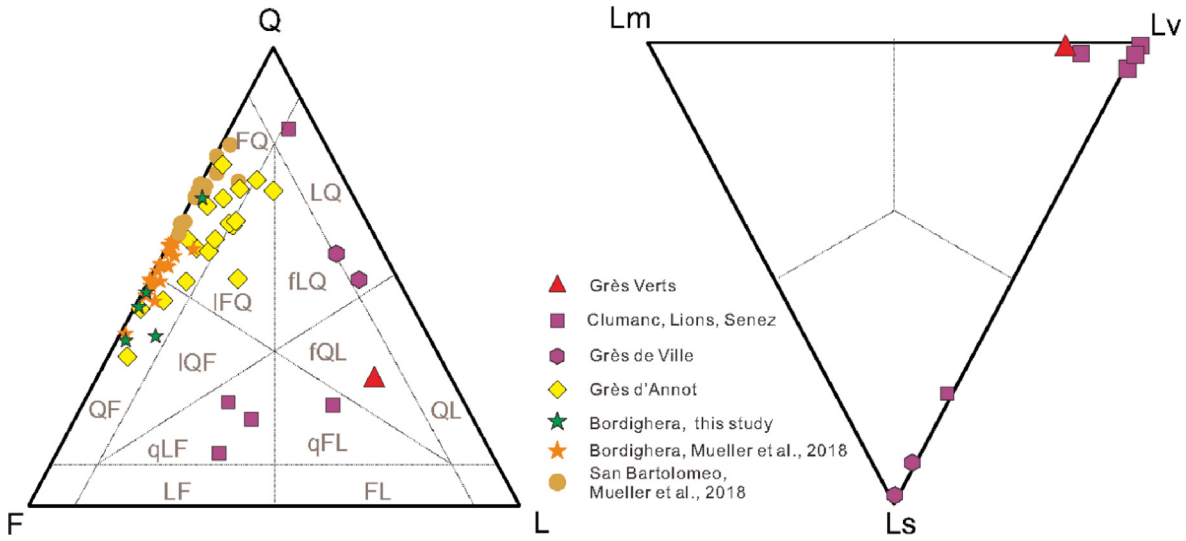

Fig. 10 Petrographic classification of the Upper Cretaceous to Oligocene sandstones of the Western Alps. Q-quartz; F-feldspar; L-lithic fragments; Lm-metamorphic lithics, Ls-sedimentary lithics; Lv-volcanic lithics.

and Garzanti, 2012), then it is very unlikely that the flexural bulge generated by the load of such an underdeveloped orogen could represent a more relevant source than the orogen itself.

Several lines of evidence should be considered. Firstly, flexural uplift could have occurred only after deposition of the youngest pelagic limestones underlying the unconformity, dated as late Maastrichtian. Secondly, sandstone detrital modes in the San Bartolomeo (average QtFL 69:29:2; 12 samples) and overlying Bordighera formations (average QtFL51:47:2; 19 samples) are similar (see Fig. 5 in Müller *et al.*, 2018), both indicating provenance from a continental block (Dickinson and Suczek, 1979). Bordighera sandstones have a higher feldspar/quartz ratio (Müller *et al.*, 2018), but age spectra of detrital zircons are the same, indicating a largely unchanged source area during the Cretaceous. Thirdly, detrital modes and age spectra of detrital zircons in the Bordighera and Annot sandstones are very similar, pointing to a source similarly including Variscan and post-Variscan granitoids and subordinate felsic volcanic rocks. Paleocurrent directions in the Grés d'Annot indicate that their source was represented by the Maures-Estérel Massif and/or Corsica-Sardinia block to the south (Joseph *et al.*, 2012). Annot turbidites were thus derived from the Maures-Estérel Massif and the Corsica-Sardinia block in the south, rather than from the proto-Alpine orogenic belt in the east.

Before the Corsica-Sardinia block started to detach itself from southern Europe in the Oligocene, this southern area including the Maures-Estérel Massif shed detritus to all sandstone units of the Barrême Basin, as suggested by dominantly Variscan and post-Variscan zircon ages (Evans and Mange-Rajetzky, 1991; Joseph and Lomas, 2004). The provenance of these units, however, was distinct in several respects. As a notable difference with the Grès d'Annot, all sandstones in the Barrême Basin yielded zircon grains dated as 29—38 Ma (i.e., close to the depositional age), testifying to penecontemporaneous magmatism in the source area. Felsic volcanic rock fragments are most abundant in the Conglomérats de Clumanc and in the Conglomérats de Saint-Lions, pointing to a source area characterized by active volcanism and possibly also by less extensively dissected Permian ignimbrites. It is worth noting that volcanism at those times is documented both by basaltic andesites to dacites, emplaced mostly in the Agay-Estérel area of southern France (41-20 Ma), and by basalts to dacites and rhyolites in Sardinia (38-15 Ma) (Lustrino *et al.*, 2017).

The abundant limestone rock fragments, especially in the Grès de Ville, suggest a local supply from Cretaceous strata. The Grès de Ville, therefore, cannot be considered as the feather-edge equivalent to the Annot Sandstone, in agreement with Evans *et al.* (2004).

The Série des Grès Verts is characterized by mid-Jurassic zircon ages and cellular serpentinite grains indicative of provenance from mantle rocks that did not undergo subduction-related metamorphism (Garzanti *et al.*, 2002). Although ophiolites are widely exposed in the Piemontese Zone, from northern Corsica to the Western Alps, most of them have undergone eclogite-facies metamorphism during the Eocene

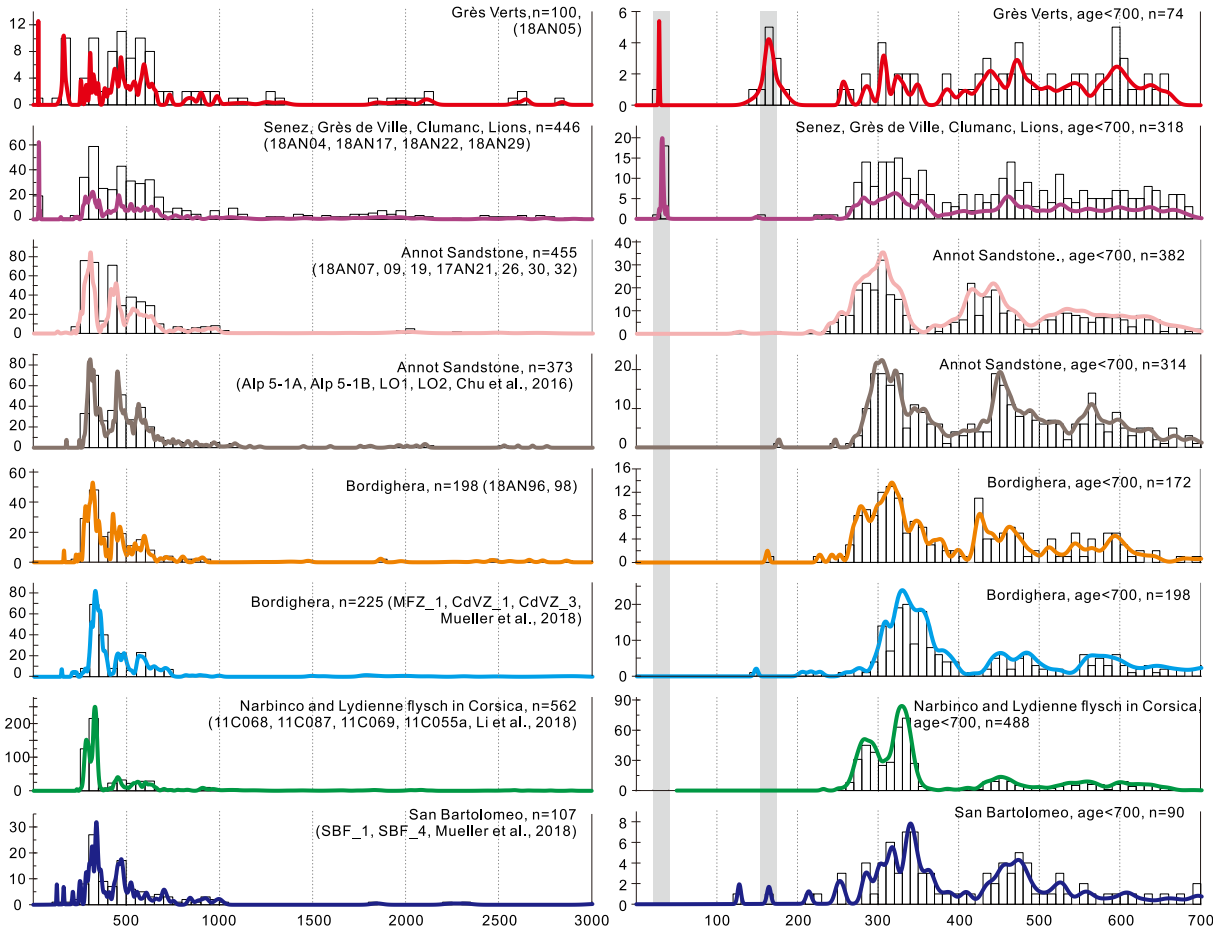

Fig. 11 U—Pb age spectra of detrital zircons contained in the Bordighera Sandstone (this study and Müller *et al.*, 2018), San Bartolomeo Formation (Müller *et al.*, 2018), Upper Cretaceous-Eocene Narbinco and Lydienne flysches in Corsica (Lin *et al.*, 2018), Eocene to Oligocene Grès d'Annot sandstone in the Annot type area (Chu *et al.*, 2016 and this study), and Oligocene to Miocene sandstones in the Barrême Basin (this study).

subduction (Rubatto *et al.*, 1998). The mantle rocks that supplied ultramafic detritus to the Sèrie des Grès Verts, instead, were part of an obducted complex analogous to the Chenaillet ophiolite (Li *et al.*, 2013). This issue is discussed in detail by Jourdan *et al.* (2012) and Schwartz *et al.* (2012), who inferred a much wider distribution of Chenaillet-type ophiolites in the Alpine orogenic prism during the Oligocene and traced the source of ophiolitic detritus reaching the Barrême Basin to an area in the NE (Briançonnais Zone, SE of the Pelvoux Massif) undergoing tectonic uplift and topographic growth in the Late Oligocene/Early Miocene. Non-subducted ophiolites, however, are also known from northern Corsica (Balagne Nappe; Marroni and Pandolfi, 2003), representing a plausible alternative source of ultramafic detritus.

In summary, and being consistent with previous paleocurrent and heavy-mineral research in the region, our provenance data indicate a southern source for the Annot Sandstone, including the Maures-Estérel Massif and the Corsica-Sardinia block (Evans *et al.*, 2004; Joseph *et al.*, 2012). The younger clastic units in the Barrême Basin point to a more complex provenance pattern, including sources within the growing Alpine orogen (Evans and Elliott, 1999). However, the exact location of Alpine orogenic sources, including non-metamorphic ultramafic detritus, is not ascertained. The overall similarity of zircon-age spectra in all studied stratigraphic units suggests that a southern area, including the Corsica-Sardinia block, may have represented the major source of detritus throughout the Oligocene.

8. Discussion

The Calcaires à Nummulites, the Marnes Bleues, and the Grès d'Annot – forming the so called "*underfilled trinity*" by Sinclair (1997) – are widely

considered to represent an archetype of foreland-basin evolution, documenting a deepening trend from shallow-marine to pelagic and eventually turbiditic deposition caused by flexural subsidence under the load of the growing Alpine orogen (Allen *et al.*, 1991, 2001; Ford and Lickorish, 2004). This succession is separated from the underlying pelagic strata of the European passive margin by a major unconformity, corresponding to a time gap of at least ~25 myr. This unconformity was generally interpreted as the result of erosion over a forebulge generated by flexural uplift of the European margin, whereas the overlying sequence (the "*underfilled trinity*") was assumed to indicate transition from the forebulge depozone to the "foredeep" depozone both in the western Alpine foreland basin (Gupta and Allen, 2000) and in the North Alpine foreland basin (Allen *et al.*, 1991; Crampton and Allen, 1995).

Based on the present study, we challenge the validity of this interpretation in the Western Alps under distinct aspects, outlined here below.

1) *Stratigraphic ages*. The *underfilled trinity* model predicts a progressive development of the wedge-shaped foreland basin during foreland-ward migration of the nascent fold-thrust belt. A change from backbulge subsidence to forebulge uplift and, eventually, to "foredeep" subsidence (Crampton and Allen, 1995; DeCelles and Giles, 1996) should thus be documented by the lower European plate at younger and younger times farther away from the orogenic front. Biostratigraphic data, however, indicate that the base of the Calcaires à Nummulites is nearly synchronous across the Annot-Peira Cava-Realdo Basin in the Western Alps (Fig. 4), and accurately constrained as the SBZ17 biozone (Bartonian) in the Peyresq and Coulomp River sections of the Annot Basin, in the Peira Cava Basin, as well as in the Realdo section of the Maritimes Alps (Sztrákos and du Fornel, 2003). Only in the Barrême Basin was the base of the Calcaires à Nummulites dated as SBZ19 (late Priabonian) (Fig. S2-1). The lack of significant diachronism among those basins speaks against the foreland-basin model. The Marnes Bleues unit is consistently dated by planktonic foraminiferal and nannofossil assemblages as the P18-19 and NP21-23 biozones (Sztrákos and du Fornel, 2003). It may be noted that also the top of the Grès d'Annot (Fig. 3G) is broadly synchronous and dated by planktonic foraminiferal and nannofossil assemblages as the P18 and NP21 biozones in the Chaluty, Grand Coyer, Annot, and St. Antonin sub-basins (du Fornel *et al.*, 2004) (Fig. 4).
2) *Provenance of the Grès d'Annot*. The *underfilled trinity* model dictates that the nascent orogen feeds detritus into the adjacent foreland basin, where tectonic subsidence on the elastic or visco-elastic lower plate is generated by the load of the growing thrust belt. The small forebulge feature may represent a minor additional sediment source (Jordan, 1995; Horton, 2018). Provenance analysis, however, indicates that the Grès d'Annot was not sourced from the Alpine orogen. Rather, the Grès d'Annot received detritus along strike from the south. Sediment sources were Variscan and post-Variscan granitoids and subordinately felsic volcanic rocks of the Maures-Estérel Massif and/or Corsica-Sardinia block located on the European lower plate, rather than the Alpine belt growing along the frontal edge of the Adriatic microplate.
3) *Nature of Cretaceous-Eocene unconformity*. In the *underfilled trinity* model, the Cretaceous-Eocene unconformity is related to the foreland-ward migration of the forebulge (Crampton and Allen, 1995). According to this model, the stratigraphic gap represented by the unconformity should be recorded earlier close to the orogenic front, and progressively later on across the foreland. However, the stratigraphic gap is invariably huge, spanning at least 25 myr in all studied localities, close to the mountain front and farther away. Moreover, the height of the forebulge is supposed to reach a few tens of meters only (50—200 m at most, according to DeCelles and Giles, 1996), whereas the Cretaceous-Eocene unconformity cuts down ≥300 m into the underlying strata of the Barrême Basin (Apps *et al.*, 2004).
4) *Sedimentary facies and microfacies evolution*. The previous paleodepth estimates and paleoenvironmental interpretations of the Calcaires à Nummulites were based on the presence, size, shape, and paleoecology of foraminifera (Crampton, 1992; Sinclair *et al.*, 1998). Following detailed microfacies analysis, a series of aggradational to progradational cycles was identified: 8 cycles at Chinaillon (Sinclair *et al.*, 1998), 4—6 cycles at Annot and St. Antonin, and 7 cycles at Champsaur (Crampton, 1992). This was taken as the basis for the flexural-eustatic numerical model (Allen *et al.*, 2001). However, our microfacies analysis documents a long-term deepening trend, showing no evidence of aggradational to progradational cycles (Figs. 7 and 8). Braided-river, fan-delta, coastal-plain and lagoonal sediments deposited within paleo-valleys (Poudingues d'Argens; Gupta, 1999; Apps *et al.*, 2004; Grosjean *et al.*, 2012, 2017) were followed by transgressive carbonates

documenting progressive deepening from inner to outer ramp environments (Calcaires à Nummulites). The deepening trend was completed by the hemipelagic *Globigerina* marls (Marnes Bleues) and overlying Grès d'Annot turbidites, testifying to be hemipelagic followed by deep-sea sedimentation.

5) *Extensional faulting*. The flexural foreland-basin model predicts that normal faults chiefly develop on the outer slope of the underthrusting lower plate. Syn-sedimentary normal faults are widely observed in the Eocene-Oligocene basins of the French Alps, as in the Marguareis Massif (Michard and Martinotti, 2002), Col de la Cayolle (Bouroullec *et al.*, 2004; Lansigu and Bouroullec, 2004), Annot Basin (Tomasso and Sinclair, 2004), Point Vert near Barcelonette (Buatier *et al.*, 2015), and Col de la Moutière (Pochat and Van Den Driessche, 2007). In concordance with the model, these normal faults were ascribed to flexural bending of the European plate (Sinclair, 1997; Tomasso and Sinclair, 2004). Syn-sedimentary normal faults, however, are not exclusively localized in the so-called "forebulge" zone, but are widespread across the Eocene-Oligocene basins of the French Alps. Additional evidence may come from the Barrême Basin, where olistoliths of the Upper Cretaceous pelagic limestone up to ~40 m-thick and ~250 m-long found in the Calcaires à Nummulites were emplaced as a gravity-driven submarine slide (Evans and Elliott, 1999; Marini *et al.*, 2022). Such a widespread syn-sedimentary tectonic activity documents a major phase of regional extension that speaks in favor of an extensional rift-related setting rather than of a foreland-basin setting.

8.1. What is the nature of the Eocene-Oligocene Annot and Barrême basins?

Several stratigraphic and sedimentological lines of evidence from the Eocene-Oligocene Annot and Barrême basins are consistent with deposition in an extensional/transtensional basin rather than in a flexural basin. These include: 1) widespread syn-sedimentary normal faults, which significantly controlled sediment delivery and paleogeography (Salles *et al.*, 2011, 2014); 2) NW-trending sub-basins displaying horst-and-graben structures; 3) deposition of Annot sandstones in a turbiditic basin structurally confined along NNW/SSE directions (Sinclair and Tomasso, 2002; Cunha *et al.*, 2017; Marini *et al.*, 2022); 4) deepening-upward trend from continental to coastal, shallow-marine, hemipelagic, and finally turbiditic deep-sea fan environments; 5) dominant source of Grès d'Annot siliciclastic detritus located — as documented in all studied sub-basins — within the European lower plate itself (Maures-Estérel Massif and/or Corsica-Sardinia block; see Fig. 5 in Joseph and Lomas, 2004), rather than in the Alpine orogen. Sudden rejuvenation and increased terrigenous supply from such a southern area may have been triggered by shoulder uplift along the western side of the Liguro-Provençal rift. Ultramafic detritus found in the Sèries de Grès Verts at the top of the Barrême Basin succession was derived from non-metamorphic obducted ophiolites and thus possibly from the Balagne Nappe of northern Corsica, rather than from metamorphic ophiolites now widely exposed in the internal domains of the Western Alps.

A drastic change in regional stress fields across the western Mediterranean region (Jolivet and Faccenna, 2000) took place during the late Eocene, when rift basins began to develop across the European plate (Ziegler, 1992, Fig. 1 in Dèzes *et al.*, 2004). Such a major revolution from compression associated with European-Adria convergence to widespread extension/transtension is here ascribed to a change in geodynamic polarity triggered by choking of the eastward Alpine subduction by the arrival of thicker European crust and consequent initiation of the westward Apenninic subduction (Doglioni *et al.*, 1998; Carminati *et al.*, 2012). This change in subduction polarity is constrained as early Bartonian (≥40 Ma) by the stratigraphic age of the base of the Epiligurid succession, which testifies to the onset of subduction-related subsidence of the Apennine accretionary prism (Garzanti and Malusà, 2008; Malusà and Garzanti, 2012). An early Bartonian age corresponds very closely to the age of the base of the Calcaires à Nummulites in the studied areas of SE France and W Liguria. The onset of subsidence in SE France and W Liguria is thus principally related here not to flexure of the lower European plate induced by the load of the Alpine orogen, but to regional extension on the upper plate of the Apenninic subduction. Consequently, rather than simply a part of the Alpine foreland basin, the late Eocene-Early Oligocene basins in the studied areas are here principally considered as extensional/transtensional basins located at the southern edge of the European Cenozoic rift system (Dèzes *et al.*, 2004).

Numerous geological data from the western Mediterranean region indicate that in the Gulf of Lion, Valencia trough, Alboran Sea, as well as between the Maures Massif and Corsica, rifting was well underway

by 33 Ma (Jolivet and Faccenna, 2000). Our considerations suggest that the tectonic revolution that trigged the major change in regional stress fields that ultimately led to the opening of the Liguro-Provençal Basin (Doglioni *et al.*, 1997; Gueydan *et al.*, 2017) started even earlier, close to 40 Ma.

A three-stage Palaeogene basin evolution of the Western Alps is thus envisaged (Fig. 12): a) tectonic uplift and development of the major Cretaceous-Eocene unconformity, which may be related either to the onset of Europe/Asia collision or to the initial uplift of the western shoulder of the Liguro-Provençal rift b) around 40 Ma, extensional/transtensional rift basins began to develop in SE France, on the upper plate of the nascent westward Apenninic subduction zone; c) around 34 Ma, exhumation of mantle eclogites was completed in the axial Ligurian Alps (i.e., Voltri Massif), followed by rapid subsidence and deposition of ophiolitic clastic conglomerates in the Tertiary Piedmont Basin (Malusà *et al.*, 2011; Amadori *et al.*, 2023). Accelerating retreat of the Apenninic subduction zone and associated upper-plate extension led to the detachment of Corsica-Sardinia from Europe, the opening of the Ligurian-Provençal trough, and full stepwise development of the European Cenozoic rift system (Ziegler, 1992; Dèzes *et al.*, 2004; Malusà *et al.*, 2015).

8.2. *From geological observations to models*

If the late Eocene-Early Oligocene basins of the French Alps developed chiefly by tectonic extension/transtension – rather than by flexure related to the growth of the Alpine orogenic prism – then the *underfilled trinity* model of foreland-basin deposition, proposed for the Western Alps, needs to be drastically reconsidered.

Because the Annot turbidites are not fed from the Alps, there was no "flysch" stage in the French Alps. The "flysch to molasse transition" (Sinclair, 1997), a

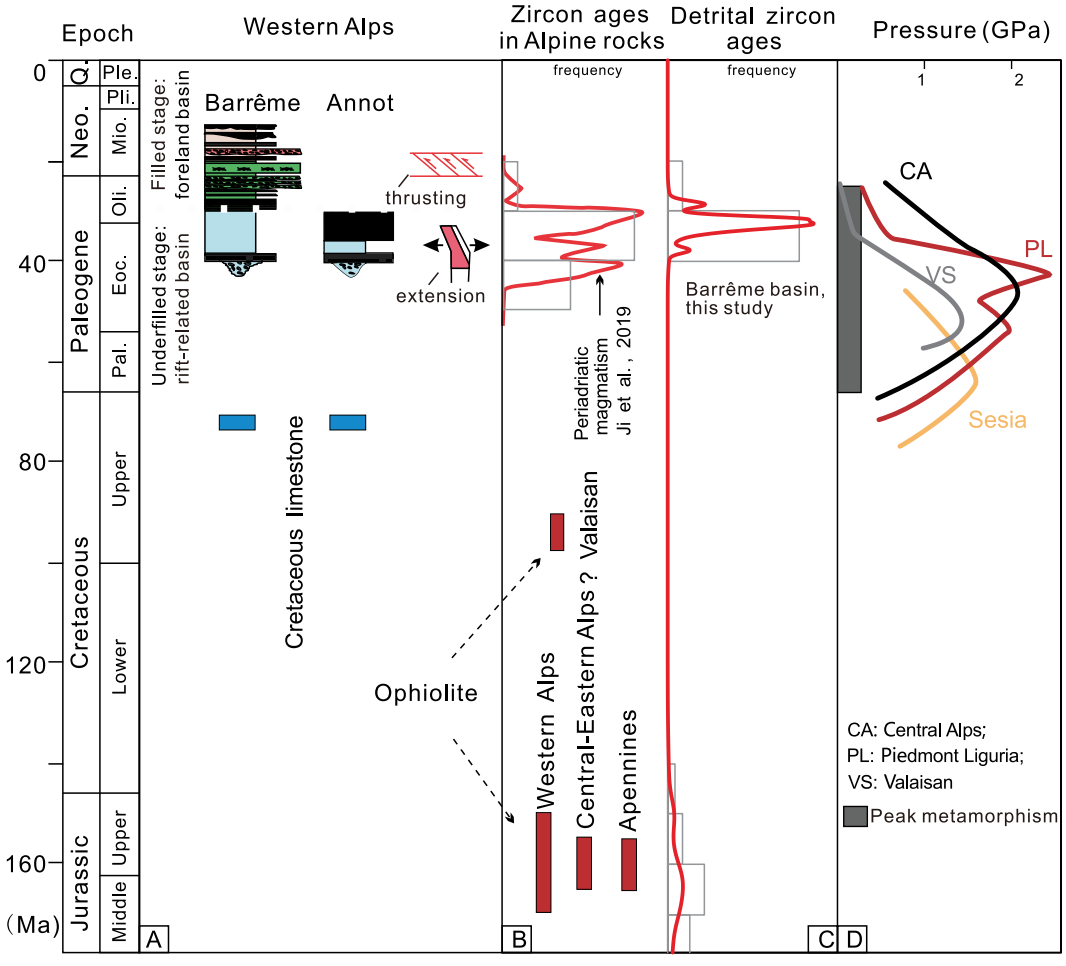

Fig. 12 Stratigraphic chart representative of the Annot and Barrême basins, showing Eocene to Oligocene rift-related deposits passing upward to foreland-basin strata. Compiled U–Pb crystallization ages from alpine ophiolites and Cenozoic Periadriatic magmatic rocks (Ji *et al.*, 2019), U–Pb ages of detrital zircons in Upper Oligocene to lower Miocene sandstones of the Barrême Basin, and schematic pressure-time (P-t) metamorphic paths of different Alpine units (modified from McCarthy *et al.*, 2018) are shown.

two-phase evolution widely applied as a dogma in foreland basins worldwide (e.g., Heller *et al.*, 1988; Allen *et al.*, 1991; Sinclair, 1997; Ford and Lickorish, 2004; Botziolis *et al.*, 2021), ceases to be meaningful. To avoid terminological confusion, the word "flysch" should be considered as a synonym of orogenic-fed remnant-ocean turbidite (as defined in Graham *et al.*, 1975; Garzanti, 2019a), and thus not applied to the Grès d'Annot in the Western Alps.

Another critical point concerns the purported implications of foreland-basin stratigraphy on the timing of collisional onset. The Cretaceous-Eocene unconformity was ascribed to flexural uplift at the start of the Alpine orogeny (Sinclair, 1997), but its nature has not been fully clarified yet. If it were related instead to rift-shoulder uplift, then the unconformity would correspond to the final choking of Alpine subduction (and consequent onset of westward Apenninic subduction), rather than to its initiation.

Lastly, our considerations lead us to ask a much more general, rather philosophical but no less important question, i.e., what are the requirements that a specific regional situation must fulfil to be translated into a "model" (Kleinhans *et al.*, 2010)? A model that in successful cases is well received and widely accepted, and eventually considered as universally valid and thus applied without much concern as a prejudicial guiding criterion while investigating analogous but not necessarily homologous geological settings. Our view is that, in recent decades, the tendency and often unavoidable necessity to overstress the significance of our research findings by forcing them beyond observations into "models" has led us to overlook the fascinating character of nature, which is the ability to surprise by presenting us with ever new, amazing phenomena (Leeder, 2011). Hypotheses including the *underfilled trinity* model and an alternative scenario proposed in this article are valid insofar they can be, and are, confronted, tested, and potentially falsified. Problems arise, instead, when unchallenged theories are used uncritically in geological investigations.

9. Conclusions

The classic Eocene-Oligocene succession of the Western Alps is here re-investigated by new field observations and stratigraphic, sedimentological, and provenance data. Based on those data, we question the tectonic nature of the Eocene-Oligocene sedimentary basins in the Western Alps. Our main results are the following:

1) *Stratigraphic ages*. Biostratigraphic data indicate that the ages of the Calcaires à Nummulites, *Globigerina* marl, and Grès d'Annot display no major diachroneity across the western Alpine foreland. The base of the Calcaires à Nummulites is accurately constrained as the SBZ17 biozone in the Peyresq and Coulomp River sections of the Annot Basin, in the Peira Cava Basin, as well as in the Realdo section of the Maritimes Alps. The top of the Grès d'Annot is also broadly synchronous and dated by planktonic foraminifera and nannofossils as the P18 and NP21 biozones in the Chaluty, Grand Coyer, Annot, and St. Antonin sub-basins.
2) *Sedimentary facies*. The major unconformity separating the uppermost Cretaceous pelagic strata from the Bartonian base of the Calcaires à Nummulites represents a 25 myr-long stratigraphic gap corresponding to the time window when the hyperextended European continental margin began to subduct beneath Adria. Deep-marine Campanian-Maastrichtian strata were abruptly overlain by the Calcaires à Nummulites, which display a long-term deepening-upward trend from a shallow-water middle ramp setting to an outer ramp episodically affected by storms.
3) *Provenance analysis*. Detrital modes, heavy-mineral assemblages, and detrital-zircon U—Pb ages show that the upper Eocene-Lower Oligocene Grès d'Annot sandstones, as well as the Upper Cretaceous Bordighera Sandstone, received detritus from Variscan and post-Variscan granitoids and subordinately felsic volcanic rocks located on the European plate rather than from the Alpine orogen. In the Barrême Basin, abundant limestone rock fragments in the Lower Oligocene Grès de Ville suggest recycling of the Cretaceous strata newly incorporated in the Alpine orogenic prism, whereas the overlying Conglomérats de Clumanc and Conglomérats de Saint-Lions were partly sourced from penecontemporaneously active volcanism, as indicated by a group of zircon grains yielding ages clustering between 29 and 38 Ma.
4) *Critique of the underfilled trinity model* (Sinclair, 1997). Based on stratigraphic ages, facies and microfacies evolution, provenance of the Grès d'Annot, and syn-depositional extensional faulting, we challenge the idea that the Calcaires à Nummulites (locally underlain by the Poudingues d'Argens), the Marnes Bleues, and the Grès d'Annot can be considered as the *underfilled trinity* of the basal western Alpine foreland basin (as in Allen *et al.*, 1991, 2001).
5) *Tectonic setting*. The stratigraphic and sedimentological evidence obtained from the Eocene-Oligocene Annot and Barrême basins supports

deposition in an extensional/transtensional, rather than purely flexural basin, during the 40-35 Ma time interval that corresponded to the initial formation and retreat of the Apenninic subduction zone, leading to upper-plate extension, detachment of Corsica-Sardinia from Europe, and full stepwise development of the European Cenozoic rift system.

Author's contributions

Xiumian Hu conceived the idea of this study, conducted the investigation and analysis process, wrote and revised the paper and was responsible for funding support of this study. Eduardo Garzanti joined in investigation and analysis process, writing, reviewing and editing of the paper. Juan Li joined in data curation, investigation, writing and editing of the paper. Marcelle BouDagher-Fadel joined in the, investigation, writing, reviewing and editing of the paper. Giovanni Coletti joined in the investigation, writing, reviewing and editing of the paper. Anlin Ma joined in data curation, writing, reviewing and editing of the paper. Wendong Liang joined in data curation, investigation, writing, reviewing and editng of the paper. Weiwei Xue joined in data curation, writing, and editing of the paper. All authors read and approved the final version of the paper.

Declaration of competing interest

The authors declare that they have no known competing financial interests or personal relationships that could have appeared to influence the work reported in this paper.

Acknowledgements

This paper is dedicated to co-authors Dr. Juan Li and Dr. Marcelle BouDagher-Fadel, who passed away while we were carrying on this work, in honor of their great love of paleontology and geology. We thank Hugh Sinclair and Marco Malusà for fruitful discussions concerning Alpine geology. We greatly appreciated the punctual critical and constructive suggestions by Andrea Di Giulio and Adrian Pfiffner on a previous version of the manuscript, and by Prof. Ian D. Somerville on this manuscript. This work is a contribution to the IGCP710. This study is financially supported by National Natural Science Foundation of China projects (91755209, 41525007).

References

Allen, P.A., Burgess, P.M., Galewsky, J., Sinclair, H.D., 2001. Flexural-eustatic numerical model for drowning of the Eocene perialpine carbonate ramp and implications for Alpine geodynamics. *Geological Society of America Bulletin*, 113, 1052—1066.

Allen, P.A., Crampton, S.L., Sinclair, H.D., 1991. The inception and early evolution of the north Alpine foreland basin, Switzerland. *Basin Research*, 3, 143—163.

Amadori, C., Maino, M., Marini, M., Casini, L., Carrapa, B., Jepson, G., Hayes, R.G., Nicola, C., Reguzzi, S., Di Giulio, A., 2023. The role of mantle upwelling on the thermal history of the Tertiary-Piedmont Basin at the Alps-Apennines tectonic boundary. *Basin Research*, 35(3), 1228—1257.

An, W., Hu, X., Garzanti, E., Wang, J.-G., Liu, Q., 2021. New precise dating of the India-Asia collision in the Tibetan Himalaya at 61 Ma. *Geophysical Research Letters*, 48, e2020GL090641.

Andersen, T., 2002. Correction of common lead in U—Pb analyses that do not report ^{204}Pb. *Chemical Geology*, 192, 59—79.

Andò, S., Garzanti, E., 2014. In: Scott, R.A., Smyth, H.R., Morton, A.C., Richardson, N. (Eds.), *Raman spectroscopy in heavy-mineral studies*. Geological Society, Special Publications, London, pp. 395—412.

Apps, G., Peel, F., Elliott, T., 2004. The structural setting and palaeogeographical evolution of the Gres d'Annot Basin. In: Lomas, P.J., Lomas, S.A. (Eds.), *Deep-Water Sedimentation in the Alpine Basin of SE France*. Geological Society, London, Special Publications, London, pp. 65—96.

Beaumont, C., 1981. Foreland basins. *Geophysical Journal of the Royal Astronomical Society*, 65, 291—329.

Beavington-Penney, S.J., Racey, A., 2004. Ecology of extant nummulitids and other larger benthic foraminifera: applications in palaeoenvironmental analysis. *Earth-Science Reviews*, 67, 219—265.

Black, L.P., Gulson, B.L., 1978. The age of the Mud Tank carbonatite, Strangways Range, Northern Territory. *BMR Journal of Australian Geology and Geophysics*, 3, 227—232.

Blum, M., Martin, J., Milliken, K., Garvin, M., 2013. Paleovalley systems: Insights from Quaternary analogs and experiments. *Earth-Science Reviews*, 116, 128—169.

Bodelle, J., 1971. *Les formations nummulitique de l'arc de Castellane*. Nice. Bureau de Récherches Géologiques et Miniéres, Paris, France.

Botziolis, C., Maravelis, A.G., Pantopoulos, G., Kostopoulou, S., Catuneanu, O., Zelilidis, A., 2021. Stratigraphic and paleogeographic development of a deep-marine foredeep: Central Pindos foreland basin, western Greece. *Marine and Petroleum Geology*, 128, 105012.

BouDagher-Fadel, M.K., 2015. The Cenozoic planktonic foraminifera: The Neogene. In: BouDagher-Fadel, M.K. (Ed.), *Biostratigraphic and Geological Significance of Planktonic Foraminifera*. Newnes, London, pp. 19—260.

Boudagher-Fadel, M.K., 2018. Revised diagnostic first and last occurrences of Mesozoic and Cenozoic planktonic foraminifera. *UCL Office of the Vice-Provost Research, Professional Papers, Series*(2), 1—5.

Boulton, S.J., Robertson, A.H.F., 2007. The Miocene of the Hatay area, S Turkey: Transition from the Arabian passive margin to an underfilled foreland basin related to closure of the Southern Neotethys Ocean. *Sedimentary Geology*, 198, 93—124.

Bouroullec, R., Cartwright, J.A., Johnson, H.D., Lansigu, C., Quémener, J.-M., Savanier, D., 2004. Syndepositional faulting in the Grès d'Annot Formation, SE France: high-resolution kinematic analysis and stratigraphic response to growth faulting. In: Joseph, P., Lomas, P.J. (Eds.), *Deep-Water Sedimentation in the Alpine Basin of Se France*. Geological Society, London, Special Publications, London, pp. 241—265.

Buatier, M.D., Cavailhes, T., Charpentier, D., Lerat, J., Sizun, J.P., Labaume, P., Gout, C., 2015. Evidence of multi-stage faulting by clay mineral analysis: Example in a normal fault zone affecting arkosic sandstones (Annot sandstones). *Journal of Structural Geology*, 75, 101—117.

Callec, Y., 2001. *La déformation synsédimentaire des bassins paléogènes de l'Arc de Castellane (Annot, Barrême, Saint-Antonin)*. Ecole Nationale Supérieure des Mines de Paris, Paris. Ph.D thesis.

Callec, Y., 2004. The turbidite fill of the Annot sub-basin (SE France): a sequence-stratigraphy approach. In: Joseph, P., Lomas, S.A. (Eds.), *Deep-Water Sedimentation in the Alpine Basin of SE France*. Geological Society, Special Publications, London, pp. 111—135.

Campredon, R., 1977. Les formations paléogenes des Alpes Maritimes franco-italiennes: Société Géologique de France. *Mémoire*, 9, 199.

Carminati, E., Lustrino, M., Doglioni, C., 2012. Geodynamic evolution of the central and western Mediterranean: Tectonics vs. igneous petrology constraints. *Tectonophysics*, 579, 173—192.

Chu, Y., Lin, W., Faure, M., Wang, Q., 2016. Detrital zircon U-Pb ages and Hf isotopic constraints on the terrigenous sediments of the Western Alps and their paleogeographic implications. *Tectonics*, 35, 2734—2753.

Cohen, K.M., Finney, S.C., Gibbard, P.L., Fan, J.X., 2013. Updated. The ICS international chronostratigraphic chart. *Episodes Journal of International Geoscience*, 36, 199—204.

Coletti, G., Mariani, L., Garzanti, E., Consani, S., Bosio, G., Vezzoli, G., Xiumian, H., Basso, D., 2021. Skeletal assemblages and terrigenous input in the Eocene carbonate systems of the Nummulitic Limestone (NW Europe). *Sedimentary Geology*, 425, 106005.

Compagnoni, R., Dal Piaz, G.V., Hunziker, J.C., Gosso, G., Lombardo, B., Williams, P.F., 1977. The Sesia-Lanzo Zone, a slice of continental crust with alpine high pressure-low temperature assemblages in the western Italian Alps. *Rendiconti Societa Italian di Mineralogia e Petrologia*, 33, 281—334.

Compagnoni, R., Hirajima, T., Chopin, C., 1995. Ultra-high-pressure metamorphic rocks in the Western Alps. In: Coleman, R.G., Wang, J.G. (Eds.), *Ultrahigh Pressure Metamorphism*. Cambridge University Press, New York, pp. 206—243.

Covey, M., 1986. The Evolution of Foreland Basins to Steady State: Evidence from the Western Taiwan Foreland Basin. In: Allen, P.A., Homewood, P. (Eds.), *Foreland Basins*. International Association of Sedimentologists, Special Publication, pp. 77—90.

Crampton, S.L., Allen, P.A., 1995. Recognition of forebulge unconformities associated with early stage foreland basin development: Example from the north Alpine foreland basin. *AAPG Bulletin*, 79, 1495—1514.

Crampton, S.L.E., 1992. *Inception of the Alpine foreland basin: basal unconformity and Nummulitic Limestone*. University of Oxford, Oxford. Ph.D dissertation.

Cunha, R.S., Tinterri, R., Muzzi Magalhaes, P., 2017. Annot Sandstone in the Peïra Cava basin: An example of an asymmetric facies distribution in a confined turbidite system (SE France). *Marine and Petroleum Geology*, 87, 60—79.

Dal Piaz, G.V., Lombardo, B., 1986. Early Alpine eclogite metamorphism in the Penninic Monte Rosa-Gran Paradiso basement nappes of the northwestern Alps. In: Brown, B.W.E.E.H. (Ed.), *Blueschists and Eclogites*. The Geological Society of America, Colorado, pp. 249—265.

De Graciansky, P.C., Durozoy, G., Gigot, P., 1982. *Notice Explicative de la Feuille Digne à 1/50 000*. Bur Rech Géol Min, Orléans.

DeCelles, P.G., Giles, K.A., 1996. Foreland basin systems. *Basin Research*, 8, 105—123.

DeCelles, P.G., Kapp, P., Gehrels, G.E., Ding, L., 2014. Paleocene-Eocene foreland basin evolution in the Himalaya of southern Tibet and Nepal: Implications for the age of initial India-Asia collision. *Tectonics*, 33, 824—849.

Desmons, J., 1992. The Briançon basement (Pennine Western Alps) : mineral composition and polymetamorphic evolution. *Schweizerische Mineralogische und Petrographische Mitteilungen*, 72, 37—55.

Desmons, J., Compagnoni, R., Cortesogno, L., Frey, M., Gaggero, L., Dallagiovanna, G., Seno, S., Radelli, L., 1999. Alpine metamorphism of the Western Alps: II. High-P/T and related pre-greenschist metamorphism. *Schweizerische Mineralogische und Petrographische Mitteilungen*, 79, 111—134.

Dèzes, P., Schmid, S.M., Ziegler, P.A., 2004. Evolution of the European Cenozoic Rift System: interaction of the Alpine and Pyrenean orogens with their foreland lithosphere. *Tectonophysics*, 389, 1—33.

Di Giulio, A., 1992. The evolution of the Western Ligurian flysch units and the role of mud diapirism in ancient accretionary prisms (Maritime Alps, Northwestern Italy). *Geologische Rundschau*, 81, 655—668.

Di Giulio, A., Amadori, C., Müller, P., Langone, A., 2020. Role of the down-bending plate as a detrital source in convergent systems revealed by U—Pb dating of zircon grains: Insights from the southern Andes and western Italian Alps. *Minerals*, 10, 1—19.

Dickinson, W.R., 1974. Plate tectonics and sedimentation. In: Dickinson, W.R. (Ed.), *Tectonics and Sedimentation*. Society for Sedimentary Geology Special Publication, Tulsa, pp. 1—27.

Dickinson, W.R., Suczek, C.A., 1979. Plate tectonics and sandstone compositions. *AAPG Bulletin*, 63, 2164—2182.

Doglioni, C., Gueguen, E., Sàbat, F., Fernandez, M., 1997. The western Mediterranean extensional basins and the Alpine orogen. *Terra Nova*, 9, 109—112.

Doglioni, C., Mongelli, F., Pialli, G., 1998. Boudinage of the Alpine belt in the Apenninic back-arc. *Memorie Della Societa'Geologica Italiana*, 52, 475, 468.

du Fornel, E., Joseph, P., Desaubliaux, G., Eschard, R., Guillocheau, F., Lerat, O., Muller, C., Ravenne, C., Sztràkos, K., 2004. The southern Grès d'Annot outcrops (French Alps): an attempt at regional correlation. In: Joseph, P., Lomas, P.J. (Eds.), *Deep-Water Sedimentation in the Alpine Basin of SE France*. Geological Society, London, Special Publications, London, pp. 137—160.

Dumont, T., Schwartz, S., Guillot, S., Simon-Labric, T., Tricart, P., Jourdan, S., 2012. Structural and sedimentary records of the Oligocene revolution in the Western Alpine arc. *Journal of Geodynamics*, 56—57, 18—38.

Dunham, R.J., 1962. Classification of carbonate rocks according to depositional textures. In: Ham, W.E. (Ed.), *Classification of Carbonate Rocks*. American Association of Petroleum Geologists Memoir, Tulsa, pp. 108—121.

Embry, A.F., Klovan, J.E., 1971. A late Devonian reef tract on northeastern Banks Island, NWT. *Bulletin of Canadian Petroleum Geology*, 19, 730—781.

Evans, M.J., Elliott, T., 1999. Evolution of a thrust-sheet-top basin: The Tertiary Barreme basin, Alpes-de-Haute-Provence, France. *Geological Society of America Bulletin*, 111, 1617—1643.

Evans, M.J., Elliott, T., Apps, G.M., Mange-Rajetzky, M.A., 2004. The Tertiary Gres de Ville of the Barreme Basin: feather edge equivalent to the Gres d'Annot? In: Lomas, P.J., Lomas, S.A. (Eds.), *Deep-Water Sedimentation in the Alpine Basin of SE France*. Geological Society, Special Publications, London, pp. 97—110.

Evans, M.J., Mange-Rajetzky, M.A., 1991. The provenance of sediments in the Barrême thrust-top basin, Haute-Provence, France. In: Morton, A.C., Todd, S.P., Haughton, P.D.W. (Eds.), *Developments in Sedimentary Provenance Studies*. Geological Society, Special Publications, London, pp. 323—342.

Féraud, G., Ruffet, G., Stéphan, J., Lapierre, H., Delgado, E., Popoff, M., 1995. *Nouvelles données géochronologiques sur le volcanisme paléogène des Alpes occidentales: exist'nce d'un événement magmatique bref généralisé. Magmatismes dans le Sud-Est de la France*, pp. 25—26. Nice.

Flügel, E., 2010. Microfacies and Archaeology. In: Flügel, E. (Ed.), *Microfacies of Carbonate Rocks: Analysis, Interpretation and Application*. Springer Berlin Heidelberg, Berlin, Heidelberg, pp. 903—915.

Ford, M., Lickorish, W.H., 2004. Foreland basin evolution around the western Alpine Arc. In: Joseph, P., Lomas, S.A. (Eds.), *Deep-Water Sedimentation in the Alpine Basin of SE France*. Geological Society, Special Publications, London, pp. 39—63.

Ford, M., Lickorish, W.H., Kusznir, N.J., 1999. Tertiary foreland sedimentation in the Southern Subalpine Chains, SE France: A geodynamic appraisal. *Basin Research*, 11, 315—336.

Gaetani, M., Gnaccolini, M., Jadoul, F., Garzanti, E., 1998. Multiorder sequence stratigraphy in the Triassic system of the western Southern Alps. In: Hardenbol, J., Thierry, J., Farley, M.B., Jacquin, T., De Graciansky, P.-C., Vail, P.R. (Eds.), *Mesozoic and Cenozoic Sequence Stratigraphy of European Basins*. Special Publications of SEPM, Tulsa, pp. 701—717.

Garzanti, E., 1991. Non-carbonate intrabasinal grains in arenites; their recognition, significance, and relationship to eustatic cycles and tectonic setting. *Journal of Sedimentary Research*, 61(6), 959—975.

Garzanti, E., 2019a. The Himalayan Foreland Basin from collision onset to the present: a sedimentary—petrology perspective. In: T.P, J., Searle, M.P. (Eds.), *Himalayan Tectonics: A Modern Synthesis*. Geological Society, Special Publications, London, pp. 65—122.

Garzanti, E., 2019b. Petrographic classification of sand and sandstone. *Earth-Science Reviews*, 192, 545—563.

Garzanti, E., Andò, S., 2019. Heavy Minerals for Junior Woodchucks. *Minerals*, 9, 148.

Garzanti, E., Andò, S., Limonta, M., Fielding, L., Najman, Y., 2018. Diagenetic control on mineralogical suites in sand, silt, and mud (Cenozoic Nile Delta): Implications for provenance reconstructions. *Earth-Science Reviews*, 185, 122—139.

Garzanti, E., Ando, S., Vezzoli, G., 2006. The continental crust as a source of sand (southern Alps cross section, northern Italy). *The Journal of Geology*, 114, 533—554.

Garzanti, E., Capaldi, T., Vezzoli, G., Limonta, M., Sosa, N., 2021. Transcontinental retroarc sediment routing controlled by subduction geometry and climate change (Central and Southern Andes, Argentina). *Basin Research*, 33, 3406—3437.

Garzanti, E., Malusà, M.G., 2008. The Oligocene Alps: Domal unroofing and drainage development during early orogenic growth. *Earth and Planetary Science Letters*, 268, 487—500.

Garzanti, E., Vezzoli, G., Ando, S., 2002. Modern sand from obducted ophiolite belts (Sultanate of Oman and United Arab Emirates). *The Journal of Geology*, 110, 371—391.

Garzanti, E., Vezzoli, G., Lombardo, B., Andò, S., Mauri, E., Monguzzi, S., Russo, M., 2004. Collision-orogen provenance (western Alps): Detrital signatures and unroofing trends. *The Journal of Geology*, 112, 145—164.

Graciansky, P., Lemoine, M., Saliot, P., 1971. Remarques sur la présence de minéraux et de paragenèses du métamorphisme alpin dans les galets des conglomérats oligocènes du synclinal de Barrême (Alpes de Haute-Provence). *Comptes Rendus de l'Academie des Sciences, Paris, Série D*, 272, 3243—3245.

Graham, S.A., Dickinson, W.R., Ingersoll, R.V., 1975. Himalayan-Bengal model for flysch dispersal in the Appalachian-Ouachita system. *Geological Society of America Bulletin*, 86(3), 273—286.

Grosjean, A.-S., Pittet, B., Ferry, S., Maheo, G., Gardien, V., 2012. Reconstruction of Tertiary palaeovalleys in the South Alpine Foreland Basin of France (Eocene-Oligocene of the Castellane arc). *Sedimentary Geology*, 275, 1—21.

Grosjean, A.-S., Pittet, B., Gardien, V., Leloup, P.-H., Mahéo, G., Barraza Garcia, J., 2017. Tectonic heritage in drainage pattern and dynamics: the case of the French South Alpine Foreland Basin (ca. 45-20 Ma). *Basin Research*, 29, 26—50.

Gubler, Y., 1958. Etude critique des sources du matériel constituant certaines séries détritiques dans le Tertiaire des Alpes françaises du Sud: formation détritique de Barrême, Flysch "Grès d'Annot". *Eclogae Geologicae Helvetiae*, 51, 942—977.

Gueydan, F., Brun, J.-P., Phillippon, M., Noury, M., 2017. Sequential extension as a record of Corsica Rotation during Apennines slab roll-back. *Tectonophysics*, 710—711, 149—161.

Gupta, S., 1999. Controls on sedimentation in distal margin palaeovalleys. *Sedimentology*, 46, 357—384.

Gupta, S., Allen, P.A., 2000. Implications of foreland paleotopography for stratigraphic development in the Eocene distal Alpine foreland basin. *Geological Society of America Bulletin*, 112, 515—530.

Handy, M.R., Schmid, S.M., Bousquet, R., Kissling, E., Bernoulli, D., 2010. Reconciling plate-tectonic reconstructions of Alpine Tethys with the geological—geophysical record of spreading and subduction in the Alps. *Earth-Science Reviews*, 102(3—4), 121—158.

Heller, P.L., Angevine, C.L., Winslow, N.S., Paola, C., 1988. Two-phase stratigraphic model of foreland-basin sequences. *Geology*, 16, 501—504.

Homewood, P., Allen, P.A., Williams, G.D., 1986. Dynamics of the Molasse Basin of western Switzerland. In: Allen, P.A., Homewood, P. (Eds.), *Foreland Basins*. International Association of Sedimentologists, Special Publication, pp. 199—217.

Horton, B.K., 2018. Sedimentary record of Andean mountain building. *Earth-Science Reviews*, 178, 279—309.

Hu, X.M., Garzanti, E., Moore, T., Raffi, I., 2015. Direct stratigraphic dating of India-Asia collision onset at the Selandian (middle Paleocene, 59±1 Ma). *Geology*, 43, 859—862.

Hu, X.M., Garzanti, E., Wang, J.G., Huang, W.T., An, W., Webb, A., 2016. The timing of India-Asia collision onset - Facts, theories, controversies. *Earth-Science Reviews*, 160, 264—299.

Hubert, J.F., 1962. A zircon-tourmaline-rutile maturity index and the interdependence of the composition of heavy mineral assemblages with the gross composition and texture of sandstones. *Journal of Sedimentary Research*, 32(3), 440—450.

Huyghe, D., Castelltort, S., Mouthereau, F., Serra-Kiel, J., Filleaudeau, P.-Y., Emmanuel, L., Berthier, B., Renard, M., 2012. Large scale facies change in the middle Eocene South-Pyrenean foreland basin: The role of tectonics and prelude to Cenozoic ice-ages. *Sedimentary Geology*, 253—254, 25—46.

Ingersoll, R.V., Bullard, T.F., Ford, R.L., Grimm, J.P., Pickle, J.D., Sares, S.W., 1984. The effect of grain size on detrital modes: a test of the Gazzi-Dickinson point-counting method. *Journal of Sedimentary Research*, 54, 103—116.

Jackson, S.E., Pearson, N.J., Griffin, W.L., Belousova, E.A., 2004. The application of laser ablation-inductively coupled plasma-mass spectrometry to in situ U—Pb zircon geochronology. *Chemical Geology*, 211, 47—69.

Ji, W.Q., Malusà, M.G., Tiepolo, M., Langone, A., Zhao, L., Wu, F.Y., 2019. Synchronous Periadriatic magmatism in the Western and Central Alps in the absence of slab breakoff. *Terra Nova*, 31, 120—128.

Jolivet, L., Faccenna, C., 2000. Mediterranean extension and the Africa-Eurasia collision. *Tectonics*, 19, 1095—1106.

Jordan, T.E., 1995. Retroarc foreland and related basins. In: Busby, C.J., Ingersoll, R.V. (Eds.), *Tectonics of Sedimentary Basins*. Blackwell Science, Oxford, pp. 331—391.

Jordan, T.E., Flemings, P.B., 1991. Large-scale stratigraphic architecture, eustatic variation, and unsteady tectonism: A theoretical evaluation. *Journal of Geophysical Research: Solid Earth*, 96, 6681—6699.

Joseph, P., Callec, Y., Ford, M., 2012. *Dynamic Controls on Sedimentology and Reservoir Architecture in the Alpine Foreland Basin: A Field Guide to the Eocene-Oligocene Grès d'Annot Turbidite System of SE France*. IFP Energies Nouvelles e-books, France.

Joseph, P., Lomas, S.A., 2004. Deep-water sedimentation in the Alpine Foreland Basin of SE France: New perspectives on the Grès d'Annot and related systems—an introduction. In: Joseph, P., Lomas, S.A. (Eds.), *Deep-water Sedimentation in the Alpine Foreland Basin of SE France*. Geological Society, Special Publications, London, pp. 1—16.

Jourdan, S., Bernet, M., Schwartz, S., Guillot, S., Tricart, P., Chauvel, C., Dumont, T., Montagnac, G., Bureau, S., 2012. Tracing the Oligocene-Miocene Evolution of the Western Alps Drainage Divide with Pebble Petrology, Geochemistry, and Raman Spectroscopy of Foreland Basin Deposits. *The Journal of Geology*, 120, 603—624.

Kempf, O., Pfiffner, O.A., 2004. Early Tertiary evolution of the North Alpine Foreland Basin of the Swiss Alps and adjoining areas. *Basin Research*, 16, 549—567.

Kleinhans, M.G., Buskes, C.J., de Regt, H.W., 2010. Philosophy of earth science. In: Allhoff, F. (Ed.), *Philosophies of the Sciences: A Guide*. Blackwell Science, Oxford, pp. 213—236.

Lansigu, C., Bouroullec, R., 2004. Staircase normal fault geometry in the Grès d'Annot (SE France). In: Joseph, P., Lomas, P.J. (Eds.), *Deep-water Sedimentation in the Alpine Foreland Basin of SE France*. Geological Society, London, Special Publications, London, pp. 223—240.

Leeder, M.R., 2011. Tectonic sedimentology: sediment systems deciphering global to local tectonics. *Sedimentology*, 58(1), 2—56.

Lemoine, M., Bas, T., Arnaud-Vanneau, A., Arnaud, H., Dumont, T., Gidon, M., Bourbon, M., de Graciansky, P.-C., Rudkiewicz, J.-L., Megard-Galli, J., Tricart, P., 1986. The continental margin of the Mesozoic Tethys in the Western Alps. *Marine and Petroleum Geology*, 3, 179—199.

Lemoine, M., Tricart, P., 1986. Les schistes lustrés piémontais des Alpes Occidentales: approche stratigraphique, structurale et sédimentologique. *Eclogae Geologicae Helvetiae*, 79, 271—294.

Li, X.-H., Faure, M., Lin, W., Manatschal, G., 2013. New isotopic constraints on age and magma genesis of an embryonic oceanic crust: The Chenaillet Ophiolite in the Western Alps. *Lithos*, 160—161, 283—291.

Li, Y., Allen, P.A., Densmore, A.L., Qiang, X., 2003. Evolution of the Longmen Shan Foreland Basin (Western Sichuan, China) during the Late Triassic Indosinian Orogeny. *Basin Research*, 15, 117—138.

Lin, W., Rossi, P., Faure, M., Li, X.-H., Ji, W., Chu, Y., 2018. Detrital zircon age patterns from turbidites of the Balagne and Piedmont nappes of Alpine Corsica (France):

Evidence for an European margin source. *Tectonophysics*, 722, 69—105.
Liu, Q., Kneller, B., An, W., Hu, X., 2021. Sedimentological responses to initial continental collision: triggering of sand injection and onset of mass movement in a syn-collisional trench basin, Saga, southern Tibet. *Journal of the Geological Society*, 178, jgs2020—jgs2178.
Ludwig, K.R., 2012. *Isoplot/Ex Version 4: A Geochronological Toolkit for Microsoft Excel: Geochronology Center* (Berkeley, California, USA).
Lustrino, M., Fedele, L., Agostini, S., Di Vincenzo, G., Morra, V., 2017. Eocene-Miocene igneous activity in Provence (SE France): $^{40}Ar/^{39}Ar$ data, geochemical-petrological constraints and geodynamic implications. *Lithos*, 288—289, 72—90.
Malusà, M.G., Faccenna, C., Baldwin, S.L., Fitzgerald, P.G., Rossetti, F., Balestrieri, M.L., Danisik, M., Ellero, A., Ottria, G., Piromallo, C., 2015. Contrasting styles of (U) HP rock exhumation along the Cenozoic Adria-Europe plate boundary (Western Alps, Calabria, Corsica). *Geochemistry, Geophysics, Geosystems*, 16, 1786—1824.
Malusà, M.G., Garzanti, E., 2012. Actualistic snapshot of the early Oligocene Alps: the Alps-Apennines knot disentangled. *Terra Nova*, 24, 1—6.
Malusà, M.G., Villa, I.M., Vezzoli, G., Garzanti, E., 2011. Detrital geochronology of unroofing magmatic complexes and the slow erosion of Oligocene volcanoes in the Alps. *Earth and Planetary Science Letters*, 301, 324—336.
Manatschal, G., Bernoulli, D., 1999. Architecture and tectonic evolution of nonvolcanic margins: Present-day Galicia and ancient Adria. *Tectonics*, 18, 1099—1119.
Marini, M., Patacci, M., Felletti, F., Decarlis, A., McCaffrey, W., 2022. The erosionally confined to emergent transition in a slope-derived blocky mass-transport deposit interacting with a turbidite substrate, Ventimiglia Flysch Formation (Grès d'Annot System, north-west Italy). *Sedimentology*, 69(4), 1675—1704.
Marroni, M., Pandolfi, L., 2003. Deformation history of the ophiolite sequence from the Balagne Nappe, northern Corsica: insights in the tectonic evolution of Alpine Corsica. *Geological Journal*, 38, 67—83.
Martini, E., 1971. Standard Tertiary and Quaternary Calcareous Nannoplankton Zonation. *Proceedings of the 2nd Planktonic Conference, Roma*, 1970, 739—785.
McCarthy, A., Chelle-Michou, C., Müntener, O., Arculus, R., Blundy, J., 2018. Subduction initiation without magmatism: The case of the missing Alpine magmatic arc. *Geology*, 46, 1059—1062.
Michard, A., Martinotti, G., 2002. The Eocene unconformity of the Briançonnais domain in the French—Italian Alps, revisited (Marguareis massif, Cuneo); a hint for a Late Cretaceous—Middle Eocene frontal bulge setting. *Geodinamica Acta*, 15, 289—301.
Montenat, C., Leyrit, H., Gillot, P.Y., Janin, M.C., Barrier, P., 1999. Extension du volcanisme oligocène dans l'arc de Castellane (chaînes subalpines de Haute-Provence); Extension of Oligocene volcanics in the Castellane Arc (Haute-Provence, Subalpine domain). *Géologie de la France* 43—48.
Morton, A.C., Hallsworth, C., 2007. Chapter 7 Stability of Detrital Heavy Minerals During Burial Diagenesis. In: Mange, M.A., Wright, D.T. (Eds.), *Developments in Sedimentology*. Elsevier, pp. 215—245.
Mount, J., 1985. Mixed siliciclastic and carbonate sediments: a proposed first-order textural and compositional classification. *Sedimentology*, 32, 435—442.
Müller, P., Langone, A., Patacci, M., Di Giulio, A., 2018. Detrital signatures of impending collision: The deep-water record of the Upper Cretaceous Bordighera Sandstone and its basal complex (Ligurian Alps, Italy). *Sedimentary Geology*, 377, 147—161.
Müller, P., Langone, A., Patacci, M., Di Giulio, A., 2019. Towards a Southern European Tethyan Palaeomargin provenance signature: sandstone detrital modes and detrital zircon U—Pb age distribution of the Upper Cretaceous—Paleocene Monte Bignone Sandstones (Ligurian Alps, NW Italy). *International Journal of Earth Sciences*, 109, 201—220.
Müller, P., Patacci, M., Di Giulio, A., 2017. Hybrid event beds in the proximal to distal extensive lobe domain of the coarse-grained and sand-rich Bordighera turbidite system (NW Italy). *Marine and Petroleum Geology*, 86, 908—931.
Muttoni, G., Erba, E., Kent, D.V., Bachtadse, V., 2005. Mesozoic Alpine facies deposition as a result of past latitudinal plate motion. *Nature*, 434, 59—63.
Oberhänsli, R., Bousquet, R., Engi, M., Goffé, B., Gosso, G., Handy, M., Höck, V., Koller, F., Lardeaux, J., Polino, R., 2004. *Metamorphic Structure of the Alps*. CCGM (Commission of the Geological Maps of the World), Paris.
Pochat, S., Van Den Driessche, J., 2007. Impact of synsedimentary metre-scale normal fault scarps on sediment gravity flow dynamics: An example from the Grès d'Annot Formation, SE France. *Sedimentary Geology*, 202, 796—820.
Ravenne, C., Riche, P., Tremolieres, P., Vially, R., 1987. Sédimentation et tectonique dans le bassin marin Eocène supérieur-Oligocène des Alpes du Sud. *Revue de l'Institut Français du Pétrole*, 42, 529—553.
Rubatto, D., Gebauer, D., Fanning, M., 1998. Jurassic formation and Eocene subduction of the Zermatt—Saas-Fee ophiolites: implications for the geodynamic evolution of the Central and Western Alps. *Contributions to Mineralogy and Petrology*, 132, 269—287.
Salles, L., Ford, M., Joseph, P., Le Carlier De Veslud, C., Le Solleuz, A., 2011. Migration of a synclinal depocentre from turbidite growth strata: the Annot syncline, SE France. *Bulletin de la Societe Geologique de France*, 182(3), 199—220.
Salles, L., Ford, M., Joseph, P., 2014. Characteristics of axially-sourced turbidite sedimentation on an active wedge-top basin (Annot Sandstone, SE France). *Marine and Petroleum Geology*, 56, 305—323.
Schlunegger, F., Jordan, T.E., Klaper, E.M., 1997. Controls of erosional denudation in the orogen on foreland basin evolution: The Oligocene central Swiss Molasse Basin as an example. *Tectonics*, 16, 823—840.
Schmid, S.M., Aebli, H.R., Heller, F., Zingg, A., 1989. The role of the Periadriatic Line in the tectonic evolution of the Alps. In: Coward, M.P., Dietrich, D., Park, R.G. (Eds.), *Alpine Tectonics*. Geological Society, Special Publications, London, pp. 153—171.

Schmid, S.M., Fugenschuh, B., Kissling, E., Schuster, R., 2004. Tectonic map and overall architecture of the Alpine orogen. *Eclogae Geologicae Helvetiae*, 97, 93—117.
Schmid, S.M., Pfiffner, O.A., Froitzheim, N., Schönborn, G., Kissling, E., 1996. Geophysical-geological transect and tectonic evolution of the Swiss-Italian Alps. *Tectonics*, 15, 1036—1064.
Schumm, S.A., 1998. *To Interpret the Earth: Ten Ways To Be Wrong*, third ed. Cambridge University Press, Cambridge, UK.
Schwartz, S., Guillot, S., Tricart, P., Bernet, M., Jourdan, S., Dumont, T., Montagnac, G., 2012. Source tracing of detrital serpentinite in the Oligocene molasse deposits from the western Alps (Barreme basin): implications for relief formation in the internal zone. *Geological Magazine*, 149, 841—856.
Serra-Kiel, J., Hottinger, L., Caus, E., Drobne, K., Ferrandez, C., Jauhri, A.K., Less, G., Pavlovec, R., Pignatti, J., Samso, J.M., Schaub, H., Sirel, E., Strougo, A., Tambareau, Y., Tosquella, J., Zakrevskaya, E., 1998. Larger foraminiferal biostratigraphy of the Tethyan Paleocene and Eocene. *Bulletin de la Societe Geologique de France*, 169, 281—299.
Serra-Kiel, J., Vicedo, V., Baceta, J., Bernaola, G., Robador, A., 2020. Paleocene Larger Foraminifera from the Pyrenean Basin with a recalibration of the Paleocene Shallow Benthic Zones. *Geológica Acta*, 18, 1—69.
Sinclair, H.D., 1997. Tectonostratigraphic model for underfilled peripheral foreland basins: An Alpine perspective. *Geological Society of America Bulletin*, 109, 324—346.
Sinclair, H.D., Naylor, M., 2012. Foreland basin subsidence driven by topographic growth versus plate subduction. *Geological Society of America Bulletin*, 124, 368—379.
Sinclair, H.D., Sayer, Z.R., Tucker, M.E., 1998. Carbonate sedimentation during early foreland basin subsidence: the Eocene succession of the French Alps. In: Wright, V.P., Burchette, T.P. (Eds.), *Carbonate Ramps*. Geological Society, Special Publications, London, p. 295. -227.
Sinclair, H., Tomasso, M., 2002. Depositional evolution of confined turbidite basins. *Journal of Sedimentary Research*, 72(4), 451—456.
Stampfli, G.M., Mosar, J., Marquer, D., Marchant, R., Baudin, T., Borel, G., 1998. Subduction and obduction processes in the Swiss Alps. *Tectonophysics*, 296, 159—204.
Stanley, D.J., 1961. Etudes sédimentologiques des grès d'Annot et de leurs équivalents latéraux. *Faculté des Sciences de l*. Université de Grenoble, France, Grenoble.
Sztrákos, K., du Fornel, É., 2003. Stratigraphie, paléoécologie et foraminifères du Paléogène des Alpes Maritimes et des Alpes de Haute-Provence (Sud-Est de la France). *Revue de Micropaléontologie*, 46, 229—267.
Tomasso, M., Sinclair, H.D., 2004. Deep-water sedimentation on an evolving fault-block: the Braux and St Benoit outcrops of the Grès d'Annot. In: Joseph, P., Lomas, P.J. (Eds.), *Deep-water Sedimentation in the Alpine Foreland Basin of SE France*. Geological Society, London, Special Publications, London, pp. 267—283.
van Wagoner, J.C., Posamentier, H.W., Mitchum, R.M.J., Vail, P.R., Sarg, J.F., Loutit, T.S., Hardenbol, J., 2012. An overview of the fundamentals of sequence stratigraphy and key definitions. In: Wilgus, C.K., Hastings, B.S., Kendall, C., Ross, C.A., Van Wagoner, J.C. (Eds.), *Sea-Level Changes: An Integrated Approach*. Society for Sedimentary Geology, Special Publication, Tulsa, pp. 39—45.
Varrone, D., d'Atri, A., 2007. Acervulinid macroid and rhodolith facies in the Eocene Nummulitic Limestone of the Dauphinois Domain (Maritime Alps, Liguria, Italy). *Swiss Journal of Geosciences*, 100, 503—515.
von Blanckenburg, F., Kagami, H., Deutsch, A., Wiedenbeck, M., Oberli, F., Meier, M., Barth, S., Fischer, H., 1998. The origin of Alpine plutons along the Peri-adriatic lineament. *Schweizerische Mineralogische und Petrographische Mitteilungen*, 78, 55—66.
von Raumer, J., Abrecht, J., Bussy, F., Lombardo, B., Menot, R.-P., Schaltegger, U., 1999. The Paleozoic metamorphic evolution of the Alpine external massifs. *Schweizerische Mineralogische und Petrographische Mitteilungen*, 79, 5—22.
Wilson, J., 1975. *Carbonate Facies in Geologic History*. Springer-Verlag, Berlin, Germany.
Yu, H.S., Chou, Y.W., 2001. Characteristics and development of the flexural forebulge and basal unconformity of Western Taiwan Foreland Basin. *Tectonophysics*, 333, 277—291.
Zhang, Q.H., Willems, H., Ding, L., Grafe, K.U., Appel, E., 2012. Initial India-Asia continental collision and foreland basin evolution in the Tethyan Himalaya of Tibet: Evidence from stratigraphy and paleontology. *The Journal of Geology*, 120, 175—189.
Ziegler, P.A., 1992. European Cenozoic rift system. *Tectonophysics*, 208, 91—111.

Appendix A. Supplementary data

Supplementary data to this article can be found online at https://doi.org/10.1016/j.jop.2024.07.001, including Figures S1—S2 and Tables S1—S6. Fig. S1 Microphotographs of key fossil species, including planktonic foraminifera (Fig. S1-1) and larger benthic foraminifera (Fig. S1-2). Fig. S2 Distribution of foraminiferal assemblages in the studied stratigraphic sections: Sauzeries in the Barrême Basin (Fig. S2-1), Peyresq (Fig. S2-2), Braux in the Annot Basin (Fig. S2-3), La Rochette in the St. Antonin Basin (Fig. S2-4), and Peira Cava (Fig. S2-5). Table S1 Measured stratigraphic sections of the Calcaires à Nummulites. Table S2 Studied sandstone samples from the Western Alps. Table S3 Petrographic analysis of the studied sandstones from the Western Alps. Table S4 U-Pb ages of detrital zircons in the studied sandstones from the Western Alps. Table S5 U-Pb ages of zircon standards. Table S6 The difference of biostratigraphic age between our work and previous studies.